York University

Vertical distribution of nocturnal nitrate radical (NO_3) investigated using direct moon light differential optical absorption spectroscopy

Chemistry 4000
Research Project

Acknowledgements

The following people's contribution to this project was essential and I would like to express gratitude accordingly in the following order:

Dr. Robert McLaren

Jamie Halla

Patryk Vojtal

Ibraheem Nuaaman

Dr. Paul Delaney

Ted Rudyk

Abstract

Atmospheric measurements of nitrate radical generally detect its absorption near the visible band of 662 nm. Our DOAS instrument was modified and a technique for moon tracking was successfully developed in order to measure NO_3. The diurnal variation of atmospheric nitrate radical was measured during the winter of 2009/10 at York University (43^o 46' N - 79^o 30' W, Alt. 199 m a.s.l.). Using passive differential optical absorption spectroscopy (DOAS) and the moon as a light source, the absorption of NO_3 in the band near 662 nm was measured. We report results from 4 nights (04, 05, 29 and 30.03.2010) in a close theoretical and preliminary-estimate agreement, as well as in agreement with similar measurements during the Antarctic winter (Wagner et al., 2000). The width and the shape of the band around 662, generally demonstrated good fit results. The highest average column reported was during the night of 30/31.03.2010 ($3.6 \cdot 10^{13}$ molec cm^{-2}) with highest concentration ~ 2 hour before sunrise of $4.4 \cdot 10^{13}$ molec cm^{-2}, and lowest value ~ 3 hours after sunset on 30.03.2010.

Table of contents

List of figures and tables

Figures

Tables

1. Introduction

Human health and well-being require that air quality is considered especially nowadays that pollution continuously poses significant threat to health worldwide. Anthropogenic emission of various gases and formation of aerosol particles contribute to air pollution (Monks et al., 2009; Fowler et al., 2009). Pollutants can reach concentrations high enough to considerably impact humans, plants, ecosystems and other life forms. Thus air quality has implications for many contemporary issues.

Today major trace gas constituents that contribute to worsening of air quality include nitrogen oxides (NO_x), SO_2, CO, O_3, as well as volatile organic compounds (VOCs) and particulate organic matter (PM, 1nm - 10μm), particularly $PM_{2.5}$ which has impact on visibility degradation, climate perturbation and human health (Liu et al., 2008).

Since the beginning of 19^{th} century the field of atmospheric chemistry has continually undergone development. Rapid growth has been observed in the development of methods and techniques for investigation of the chemistry of Earth's atmosphere. One such technique is differential optical absorption spectroscopy (DOAS), originally introduced in the late 70s (Platt et al., 1979).

1.1. Night time chemistry of NO_3

Although in a very low concentrations (ppt), radical species such as NO_3 and OH can trigger important chemistry in the atmosphere and especially in the troposphere during night. However nocturnal chemistry dominated by NO_3 in the polluted urban boundary layer has received surprisingly little attention thus far.

Nitrate radical is an important species for the oxidation of volatile organic compounds (VOCs) and hydrocarbons during the night. This aligns NO_3 among the most important species for the cleaning efficiency of the troposphere. NO_3 plays a major role in atmospheric aerosol formation that has an important impact on visibility degradation and climate change. Both the nocturnal budget of nitrogen oxides (NO_x where $NO_x = NO + NO_2$) and volatile organic compounds (VOCs) are influenced by NO_3 where NO_x and VOC amounts influence the composition of aerosols and levels of air pollutants in urban areas (Stutz et al., 2009). Furthermore, it has been shown that NO_3 is a potential sink for NO_x near the surface, but a reservoir for NO_x aloft (Wang et al., 2006; Brown et al., 2007). Knowledge of the vertical distribution of NO_3 is important since it is a key to catalysis in the complex night-time atmospheric chemical system. Studies have shown that NO_3 may play an important role in the formation of secondary organic aerosols (McLaren et al., 2004).

Nitrate radical is present in significant amounts only during night. Radiation absorption in the visible solar spectrum decomposes NO_3 during the day to NO_2 and O (^3P) by R3 and to a lesser extent by R3b . Formation of NO_3 requires the consumption of O_3 according to reactions R1 and R2 (Noxon et al., 1980; Weaver et al., 1996). Presence of the stable N_2O_5 species leads to lower amounts of NO_3 but the stability of these species can be overcome thermally to produce more NO_3 (R5). The nitrate radical can react to form N_2O_5 when NO_2 is available in the

troposphere and thus be stored in the form of reservoir species (R4). It follows that NO_3 is mainly derived from anthropogenic NO_x sources, primarily fossil fuels burning, technological sources and transportation (Table 1).

$NO + O_3 \rightarrow NO_2 + O_2$	(R1)	titration reaction
$NO_2 + O_3 \rightarrow NO_3 + O_2$	(R2)	
$NO_3 + h\nu \rightarrow NO_2 + O\ (^3P)$	(R3)	$\lambda_1 < 580$ nm (photolysis)
$NO_3 + h\nu \rightarrow NO + O_2$	(R3b)	$\lambda_2 < 700$ nm (photolysis)
$NO_2 + NO_3 \rightarrow N_2O_5$	(R4)	
$N_2O_5 \rightarrow NO_2 + NO_3$	(R5)	thermal reaction
$N_2O_5 + H_2O_{(g)} \rightarrow 2HNO_{3(g)}$	(R6)	
$NO_3 + RH \rightarrow R\cdot + HNO_3$	(R7)	
$NO_3 + NO \rightarrow NO_2 + NO_2$	(R8)	

Table 1. Global emission of NO_x as determined in 1997 (Muller et al., 2005). NO_x budgets are given in TgN/yr

Species	Sources			Total
Nitrogen Oxides (NO_x)	Anthropogenic	Technologial	24.6	30.89
		Biofuels	2.41	
		Ships	2.92	
		Aircrafts	0.64	
		Agr. waste burning	0.62	
	Vegitation fires	Savanna	5.19	6.88
		Tropical forests	1.47	
		Non-tropical	0.22	
	Soils			8
	Lightning			3
				48.77

In freshly polluted air masses NO_3 is quickly destroyed in a reaction with NO (R8). In the nocturnal boundary layer (NBL), NO_3 and N_2O_5 equilibrate quickly unless NO_2 levels are very

low (Smith et al., 1990; Smith et al. 1993; Sommariva et al., 2007) and thus R4 becomes sink for NO_3. Since N_2O_5 is directly linked to concentrations of NO_3, it is worth mentioning that it leads to the production of HNO_3 through heterogeneous reaction with H_2O by R6. Both NO_3 and N_2O_5 are uptaken on aerosols. General reaction of NO_3 with VOCs, e.g. isoprene, terpenes, alkenes, aldehydes and aromatic is given by R7. Alkyl radicals generated by R7 are unstable and tend to form peroxy radicals that further transforme into stable organic nitrates or carbonyl compounds.

1.2. NO_3 link to important chemistry

Dinitrogen pentoxide is an important intermediate that can be linked to important chemical mechanisms taking place in the nocturnal troposphere. Studies (McLaren et al., 2004) have indicated that NO_3 amounts can be attributed to formation of secondary organic aerosols via the formation of N_2O_5. Indeed most of the measured fine particle nitrate produced over night from N_2O_5 hydrolysis. N_2O_5 can react heterogeneously (R9) with H_2O to form particulate HNO_3 which can either be dry deposited or react with NH_3 to form particulate ammonium nitrate (R10).

$$N_2O_5 + H_2O_{(p)} \rightarrow 2HNO_{3(p)} \qquad \text{(R9)}$$

$$HNO_3 + NH_3 \rightarrow NH_4NO_3 \qquad \text{(R10)}$$

In coastal urban regions where NaCl and HCl are available, subsequent reactions of N_2O_5 can lead to the formation of photolabile species such as ClNO, $ClNO_2$, Cl_2 which accumulate overnight and can release Cl radical on the next day. Enhanced O_3 formation observed near coastal urban regions is likely attributed to this source of Cl radical (McLaren et al., 2009). The formation and amounts of N_2O_5 at night is largely dependent on the amounts of NO_3 present and hence it is important to further our knowledge on NO_3 vertical profiles in urban polluted areas.

1.3. Objective

Recent report (Brown et al., 2007) on urban NO_3 concentrations within the nocturnal boundary layer (NBL) and up to 300 m altitude, suggested that NO_3 mixing ratio is as high as 40-80 ppt. Other studies (Noxon et al., 1979; Solomon et al., 1989; Wagner et al. 2000) used direct moonlight observations to demonstrate that vertical NO_3 concentrations can vary from $2 \cdot 10^{13}$ molec cm^{-2} to $1 \cdot 10^{14}$ molec cm^{-2}. Based on kinetic data from Jet Propulsion Laboratories (JPL, 1997), we have estimated that vertical concentrations of NO_3 above 300 m in urban areas can be as high as $1 \cdot 10^{13}$ molec cm^{-2}, and hypothesized even higher concentration. Given this information, our primary objective was to try out a direct moonlight DOAS observation in order to measure NO_3 and obtain information on how it is distributed vertically in the troposphere and the stratosphere.

2. Theory

2.1. Differential optical absorption spectroscopy

Atmospheric trace gasses can be found in abundances as low as ppt or ppb levels. This requires highly sensitive measurement technique with very low detection limits. Such techniques must not be influenced either negatively or positively by any other constituents present simultaneously with the investigated ones. Differential optical absorption spectroscopy (DOAS) fulfils these requirements.

The DOAS techniques was developed in the university of Heidelberg, Germany, and first used in the late 70s (Platt et al., 1979). It follows the Beer-Lambert absorption law:

$$I(\lambda) = I_o(\lambda)\,\mathrm{e}^{(-L\sigma(\lambda)c)} \tag{1}$$

where $I_o(\lambda)$ is the originating radiation intensity from a light source, $I(\lambda)$ is the radiation intensity that passes through a volume of air with thickness L in which the species to be measured are present at a concentration c (Fig. 1) . The absorption cross section of the species is wavelength dependent and is denoted by σ(λ) which can be measured in laboratory settings.

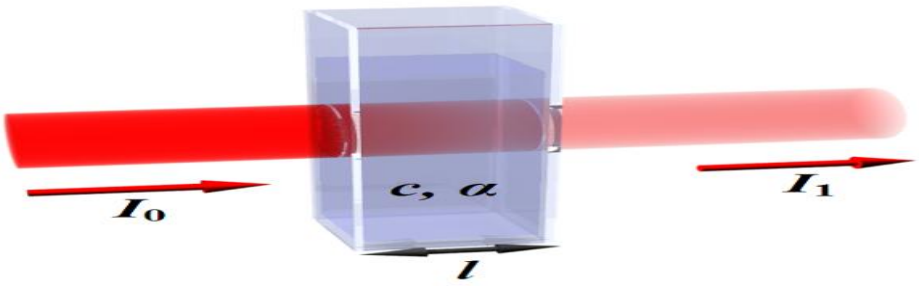

Figure 1. Beer-Lambert law. The originating light intensity is attenuated as it passes through a layer of absorbers.

The ratio of $I_o(\lambda)/ I(\lambda)$ can be calculated and therefore be used to estimate the concentration of the gas absorber of interest. Therefore the concentration is given by:

$$c = \frac{D}{(\sigma(\lambda)L)} \tag{2}$$

where D is the total optical density of the probed air volume or the natural logarithm (*ln*) of the ratio of $I_o(\lambda)/ I(\lambda)$. However, processes that take place in the atmosphere are not the same as in the lab. This means that the incoming light is attenuated from its original intensity due to various scattering process that take place. Therefore when using absorption spectroscopy in the atmosphere, an account for Rayleigh scattering (scattering by air molecules) and Mie scattering (scattering due to atmospheric aerosols) must be given. Hence the original Beer-Lambert law applied to atmospheric absorbers will take the following form:

$$I(\lambda) = I_o(\lambda)\, \mathrm{e}^{[-L(\Sigma\sigma_i(\lambda)c_i)+\varepsilon_R(\lambda)+\varepsilon_M(\lambda)]} \tag{3}$$

where $\varepsilon_R(\lambda)$ term accounts for Rayleigh scattering and $\varepsilon_M(\lambda)$ for Mie scattering. The whole modified equation includes a sum for all trace gases in the investigated air volume.

In practice however two major problems are observed that require resolution. One problem is that overlapping by several species may take place in a region of a spectrum. The second problem requires that $I_o(\lambda)$ is determined. An elegant approach has been developed that requires division of the incoming radiation into slow and rapidly varying spectral components (Platt, 1994). This is the so-called differential absorption which separates these different contributions into slow ($\sigma_{io}(\lambda)$) and rapidly ($\sigma_i`(\lambda)$) varying components with wavelength (λ):

$$\sigma_i(\lambda) = \sigma_{iO}(\lambda) + \sigma_i^{'}(\lambda) \tag{4}$$

In analogy the total differential optical density D` can be defined and since there is only concern with the differential cross section of the absorbers of interest, then D` is given by:

$$D' = \log \frac{I_o(\lambda)}{I(\lambda)} = L \sum (\sigma_i'(\lambda) c_i) \tag{5}$$

The idea used by differential absorption spectroscopy is well illustrated on Fig. 2 where it can be seen the well-defined difference between the originating true light intensity and the one that reaches the detector after passing through a layer of absorbers.

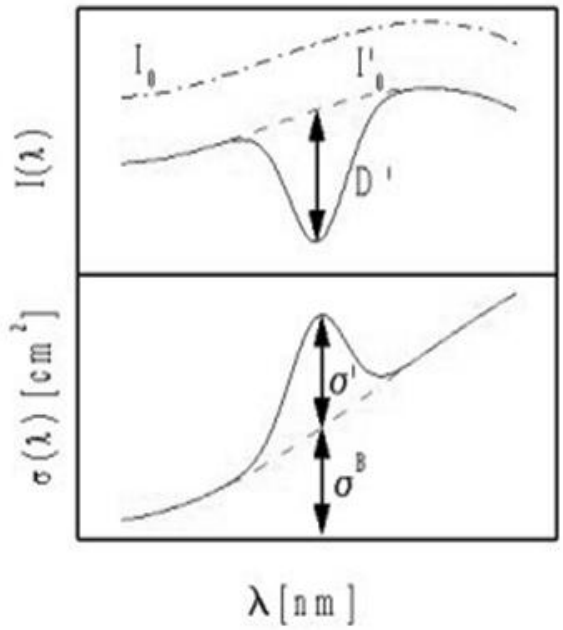

Figure 2. DOAS. Top panel: the dashed line, *I(λ)*, represents the radiation intensity that reaches the detector. The solid line, $I_o(\lambda)$, is the intensity of a narrow absorption of species (Platt and Perner, 1983; Platt, 1994). Bottom panel: same analogy applies to the differential cross sections of trace absorbers.

DOAS has a great advantage in the unequivocal detection of a trace gas due to detection of extremely low absorptions (D`~10^{-4}). Properties of this type are characteristic for a powerful elucidation techniques one of which is differential spectroscopy.

2.1.1. Ground-based active DOAS

Active instruments based on UV absorption have been designed in a large variety of ways (Platt and Stutz, 2008). The most common variation of DOAS consists of artificial (active) light source and receiving system where the two are separated by a well-defined distance in the range of few hundred meters to several kilometres (Fig. 3). This set-up is known as single pass DOAS since the light is received directly by a spectrometer after travelling well-known path. The

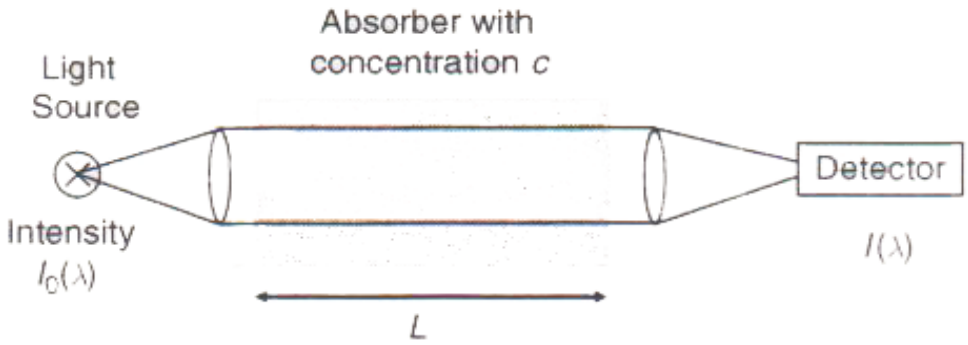

Figure 3. Single pass active DOAS. A beam of light passes through an air volume that contains the absorbers of interest. A well-known distance separates the detector from the light source (Platt, 2008; p. 137).

technique is especially useful for the measurement of unstable tropospheric species such as OH radical and NO_3. A variation of this technique makes use of a retro-reflector located at a well known distance – dual pass DOAS which has the advantage of increased path length and therefore lower detection limit (Fig. 4). The active light source used in these cases is typically a xenon (Xe) arc lamp that emits UVA to UVC light and essentially smooth spectrum in the useful spectral range (Yu et al., 2004; Zingler and Platt, 2005). Other light sources are known and used in practice, such as lasers and optical elements adapting the absorption path of the light source and the spectrometer (Brandenburger et al., 1998).

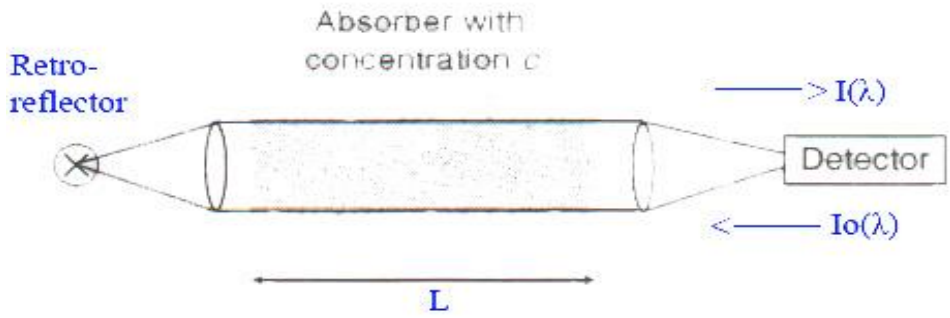

Figure 4. Dual pass active DOAS. A beam of light passes through an air volume twice as the light originates from the point where the detector is. A well-known distance separates the detector from the retro-reflector.

2.1.2. Passive multi axis (MAX) DOAS

While an active DOAS system is developed mainly for tropospheric measurements, a passive system arranges itself among the important ones for ground-based measurements during the day and the night. The greatest advantage of MAX DOAS is that it can utilize scattered light from multiple viewing directions, i.e. there is no need of a retroreflector, and therefore used to retrieve vertical profiles of trace gases.

In comparison to active DOAS, passive requires a much less sophisticated optical system. In return MAX DOAS is capable of yielding troposhperic and stratospheric profiles of OClO, BrO, IO, NO_2, SO_2, NO_3 and other constituents (Noxon et al., 1980; Weaver et al., 1996).

The system consists of a telescope assembly with a primary mirror pointed at a point of a scattering process in the atmosphere (Fig. 5). Measurement of this type requires an understanding of complex phenomena such as radiative transfer, air mass factor (AMF) and transport phenomena (Solomon, 1987; Platt et al., 1997). In this case the measured quantity of the gas is not the concentration, but the slant column density (SCD):

$$SCD = S = \int_0^L c(s)ds \tag{6}$$

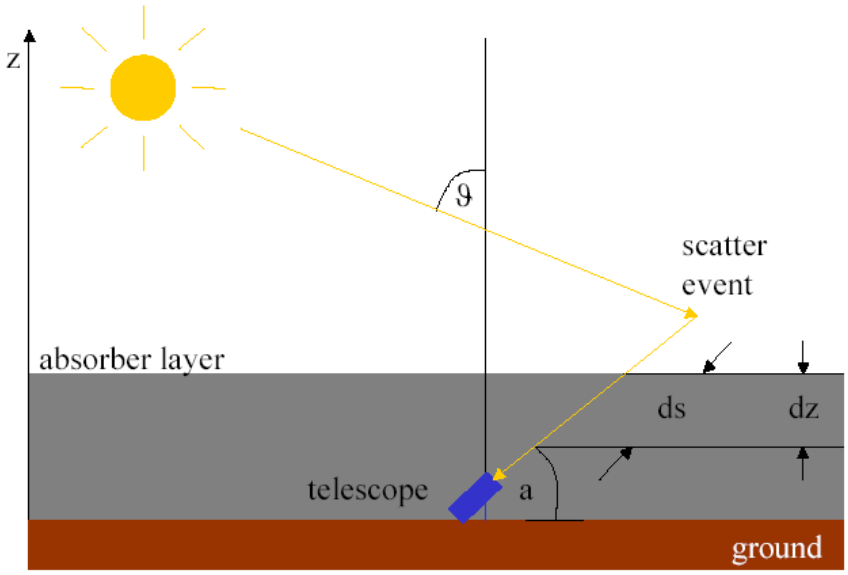

Figure 5. MAX-DOAS. Scattering can be observed at variable angles (0 – 90°) and then information be combined for all different observations (Platt, 2008; p. 341).

DOAS is generally interested in the differential SCD as explained previously. In order to obtain the vertical column density (VCD) for an absorber, an AMF must be used. AMF has been used for many years for interpreting scattered light (Solomon, 1987). Given than the VCD is:

$$VCD = V = \int_0^\infty c(z)dz \tag{7}$$

measured vertically to the surface of the Earth. Then the AMF is defined as:

$$AMF = \frac{DSCD}{VCD} \tag{8}$$

where DSCD is the differential slant column density of the absorbers and VCD is the true vertical column of the species measured (Honninger et al, 2004).

2.1.3. Direct moon light DOAS

Direct moon light DOAS is a type of off-axis method that utilizes moon-light by directly looking at the moon to obtain a spectrum for the analysis of vertical profiles of trace gases. Geometrically this method is easier than MAX-DOAS, since the path from the moon is well-known. However one needs to consider the altitude and azimuth angles, the lunar phases and the luminescence of the moon as well as a method to track this celestial body.

Generally the incoming light intensity from stars or the moon is so low that it would be no alternative to spectroscopy during the day. However during night this method allows for useful study of photolabile species such as OClO and NO_3. A major requirement is that the moon is not obscured by clouds and it is sufficiently large. The latter requirement draws upon the fact that the incoming radiation from the moon is approximately 10% of the solar radiation although the spectra of the moon and the Sun are almost identical. Given the lowered intensity, incoming light from the moon can be significantly attenuated by any aerosol, clouds or fog on the path.

There are few significant advantages associated with this technique. First, Raman scattering (Ring effect) does not need to be considered as it does with sky scattered sunlight (Platt, 2008, p. 430). Second, the air mass factor can be estimated by:

$$AMF = \frac{1}{\cos\theta} \tag{9}$$

where θ is the angle between the viewing direction of the scope and the zenith (Fig. 6), also known as the lunar zenith angle (LZA). This approximation only holds true for LZA $<80^{o}$.

For the proper estimation of NO_3 measured by direct moon light, a few considerations

play an important role. One such consideration is the amount of NO_3 present in the reference

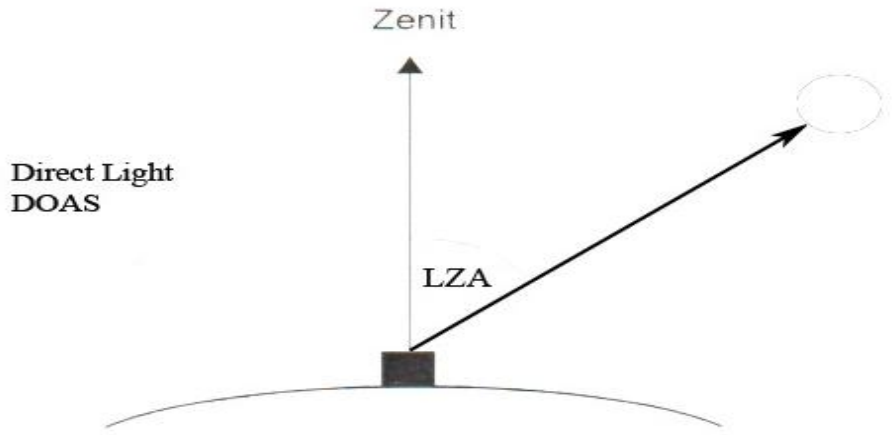

Figure 6. Direct moon light DOAS. Column densities are function of lunar zenith angle (LZA) and SCD of the measured absorber

spectrum that can be estimated by constructing a Langley plot (Solomon et al., 1989; Wagner et al., 2000) (see discussion below). Thus the true NO_3 present in the individual spectra is accounted for by:

$$VCD = \frac{(DSCD_m + DSCD_{ref})}{AMF} \tag{10}$$

where $DSCD_m$ is the measured slant column density and $DSCD_{ref}$ is the estimated slant column of the reference spectrum.

2.2. Langley Plots

Direct moonlight DOAS is a type of off-axis method that requires some AMF calculations. Atmospheric observations using zenith light have been used for a while (Solomon et al., 1987, 1989; Wagner et al., 1998, 2000). Langley extrapolations is a commonly used method for measuring the sun's radiance for purposes of removing the effect of the atmosphere. In this case it is used to estimate the slant column concentration of NO_3 present in the reference spectrum

used for the fit. The Langley method can be applied to any celestial body (e.g. moon). The Lambert-Beer's law is applied in this case:

$$\frac{I}{I_o} = e^{-m\tau} \tag{11}$$

where *m* is the geometrical factor accounting for the slant path through the atmosphere, well-known as airmass factor (AMF), and τ is the atmospheric optical depth. A major requirement for a good Langley plot is a constant atmosphere, i.e. absence of clouds and constant aerosol. Thus the AMF is calculated from modeling of the paths of the measured radiation through the atmosphere (Solomon et al., 1987).

Many formulas have been developed to fit values for airmass (Rozenberg, 1966; Young, 1994). For small and medium LZA (<70^o), the stratospheric airmass is well approximated by 1/cos(LZA) and the one in the troposphere by 1/cos(EA), where EA is the elevation angle (12). For large LZA (>80^o), the AMF depends on wavelength, vertical profiles of absorbers, atmospheric aerosols (Otten et al., 1998) as well as stratospheric and tropospheric clouds, and the error associated with estimating the AMF is large. In principle for larger zenith angles radiative transport models for direct light would have to be used.

$$AMF_{strat} = \frac{1}{\cos(LZA)} \qquad AMF_{trop} = \frac{1}{\sin(EA)} \tag{12}$$

When the zenith angle is small, a good approximation assumes a homogeneous atmosphere (ignoring curvature). The Earth is not flat, however, and this formula is useful for LZA between 0^o and 80^o due to strong Rayleigh extinction for LZA>80^o. At greater angles the accuracy

degrades rapidly. The above formula gives a maximum airmass of 40 at 88^o. From the slope (fitted line) the absorption corresponding to the vertical atmospheric absorption path is derived. For LZA between 0^o and 80^o, most of the estimated VCD_{ref} will be in the stratosphere and the $DSCD_{ref}$ will be given by:

$$DSCD_{ref} = VCD_{ref} \cdot AMF \tag{13}$$

Thus the slope of a Langley plot represents a constant vertical column that can be used to obtain the $DSCD_{ref}$.

2.3. Fraunhofer reference spectrum (FRS) and the Ring effect

Rotational Raman scattering on air molecules is responsible for the so called Ring effect. Approximately 4% of the scattered light fills-up the strong Fraunhofer lines of the solar spectrum. As a result, reduction of a few percent of the narrow absorption features occurs (Platt, 2008; pp. 329-377). Atmospheric absorbers can be more than an order of magnitude smaller compared to the Ring effect and hence accurate correction is required. Fortunately, as mentioned previously, this effect is absent with direct light measurements due to absence of scattered light resulting from Raman scattering.

Any spectrum from the sun or the moon is dominated by strong emission lines called Fraunhofer lines. These lines result from the spectral emission by various elements present at the surface of the sun. Since the moon spectrum is a reflection of the sun's spectrum but with lower light intensity, it will therefore contain these lines. Fraunhofer lines can influence trace gas characteristics and make it difficult to see an absorber. It is then necessary that a Fraunhofer reference spectrum (FRS) is included in the analysis. In order to fit the trace gas of interest, a FRS can be taken at different zenith angles, with difference in the concentration of the trace gas.

3. Experimental

3.1. Experimental set-up and location

The experimental set-up can be seen as two major assemblies – telescope and spectrometer. The telescope is a 8" diameter, 1000 mm focal length reflector Skywatcher telescope tube mounted on the German Equatorial CG-5 mount. The scope's optic system has a primary mirror used to reflect the incoming light into a smaller, secondary mirror which then reflects the light into a 1000 ± 20 μm inner diameter fibre optic cable. The Ocean Optics fibre optic cable is 2 meter long of the P1000-2-UV-VIS type, buffer-coated with acrylate.

Signal travelling through the optic cable reaches an S2000 Ocean Optic spectrometer which consists of 2048 element charge coupled device (CCD) array detector, and connects to a PC-computer via serial RS-232 port. The fast interface allows for data acquisition with integration time as fast as 3 ms. In order to keep the CCD array detector at a stable constant temperature (5.2 ^{o}C) through the campaign, a temperature controller is used. The entire assembly is schematically represented on Fig. 7 below.

Since the primary objective of this work is to investigate urban NO_3 vertical profiles of mid-latitude (43^{o} 46' N – 79^{o} 30' W), it is reasonable to choose a strategic. The location of direct moon lightDOAS for the winter of 2009/10 is shown below on Fig. 8. Fig. 9 shows exact location, over a parking lot of 199 m altitude located at York University.

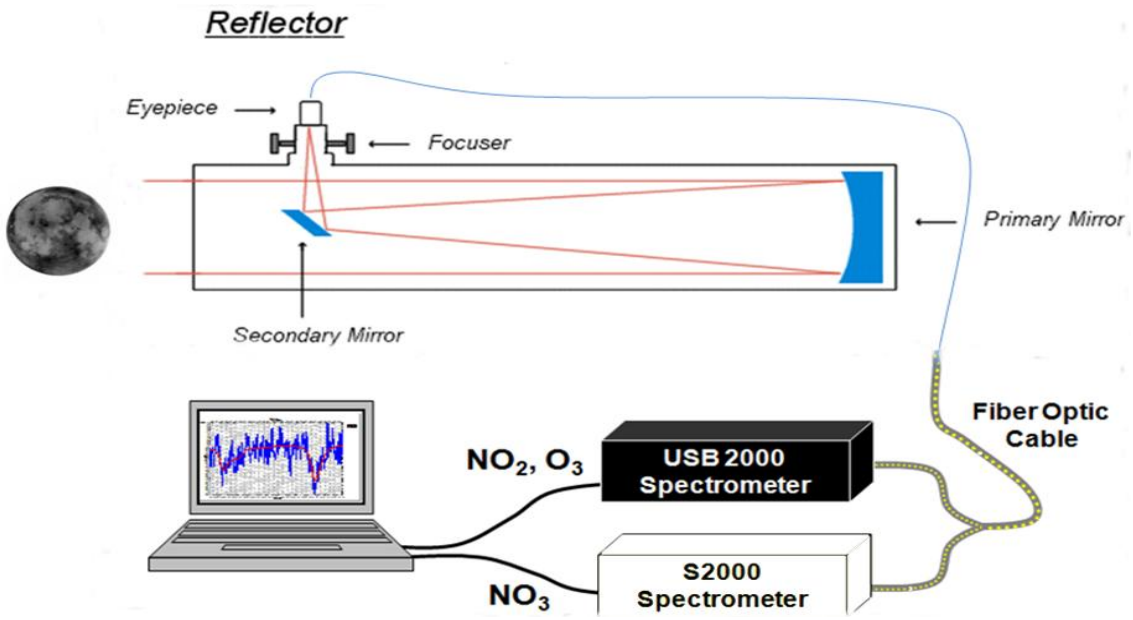

Figure 7. Experimental set-up. The telescope assembly transfers spectral data into the S2000 spectrometer. An integrated differential spectrum is obtained and stored.

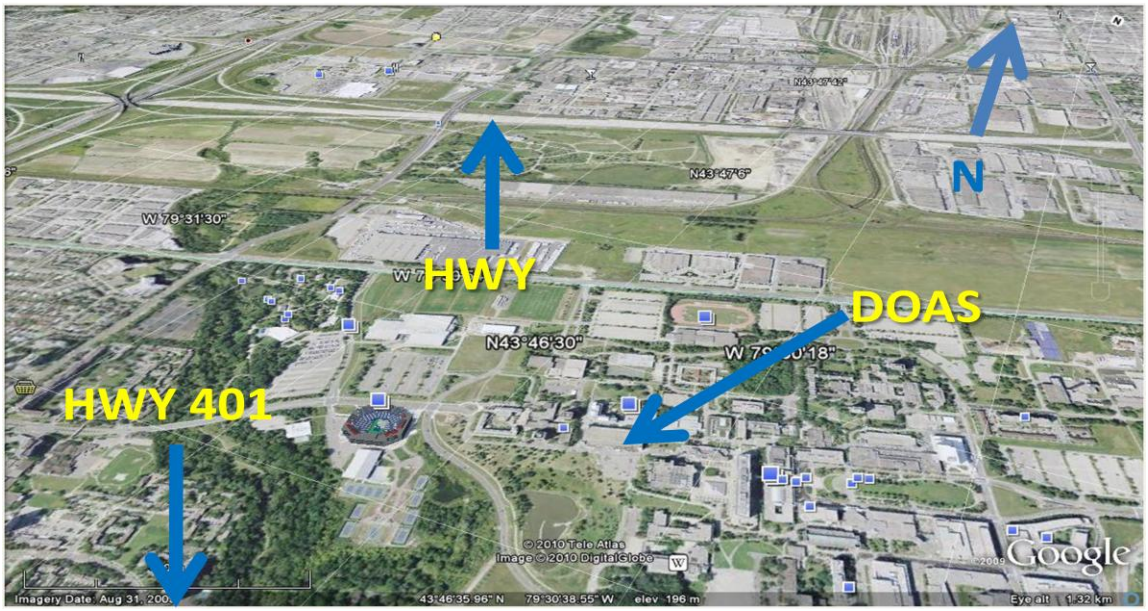

Figure 8. Experiment site. Major highways (e.g. HWY 401) are located near the observation site. Possible polluted episodes are expected.

Figure 9. Experiment location. It is important that nearby structures do not obscure the field of view. William Small garage structure is located at 43º 46’ N – 79º 30’ W, 199 m altitude.

3.2. Celestron CG-5 equatorial mount. Alignment

As mentioned previously, direct light DOAS measurements require a device that can track a celestial body continuously and accurately throughout a campaign of spectral acquisition. For this campaign we choose a heavy duty (CG-5GT) computerized German Equatorial mount. This advanced series mount is precision-accurate down to 1.5 arc-minute and suits the purpose well. Two main motors are powered by 12V power supply have the capability to slew up to a 10” diameter telescope with focal length up to 1200 mm, to any star in the built in catalogue. The Liquid Crystal Display (LCD) hand control operates in temperature range as low as -15 ^{o}C. Two major rotation axes, declination (DEC) and polar axis, offer 0-90^{o} in zenith and 0-360^{o} view in azimuth, respectively (Fig. 10).

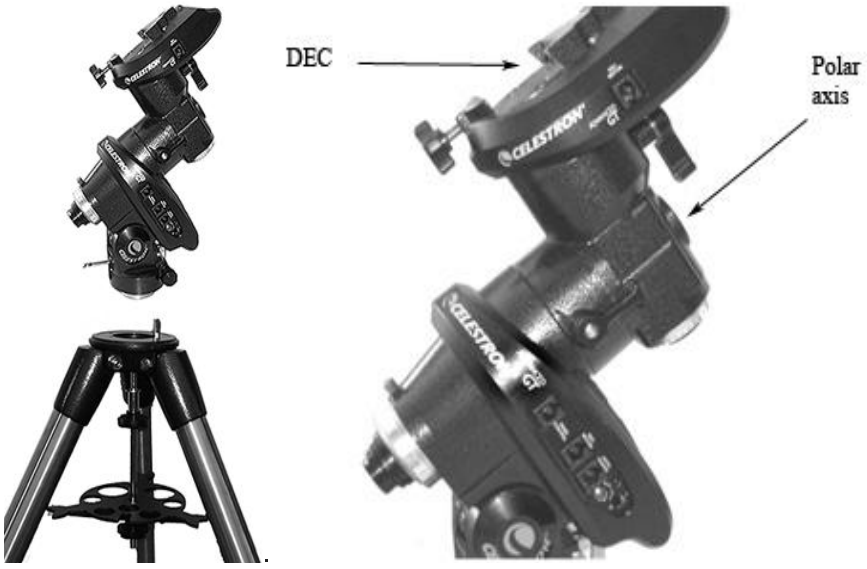

Figure 10. On the left: German Equatorial CG-5 computerized motor mount with 2" steel tripod support. On the right: shown are the declination and polar axis controlled by high precision motors.

Tracking the moon throughout night requires that the mount is aligned with at least three stars – one is to be on one side of the meridian and two on the opposite. Prior to alignment the North Celestial Pole (NCP) must be located and the mount pointed at it as precisely as possible (Fig. 11). Aligning the telescope with the NCP allows for the motors to calculate the displacement due to the rotation of Earth and thus track any celestial object in the night sky.

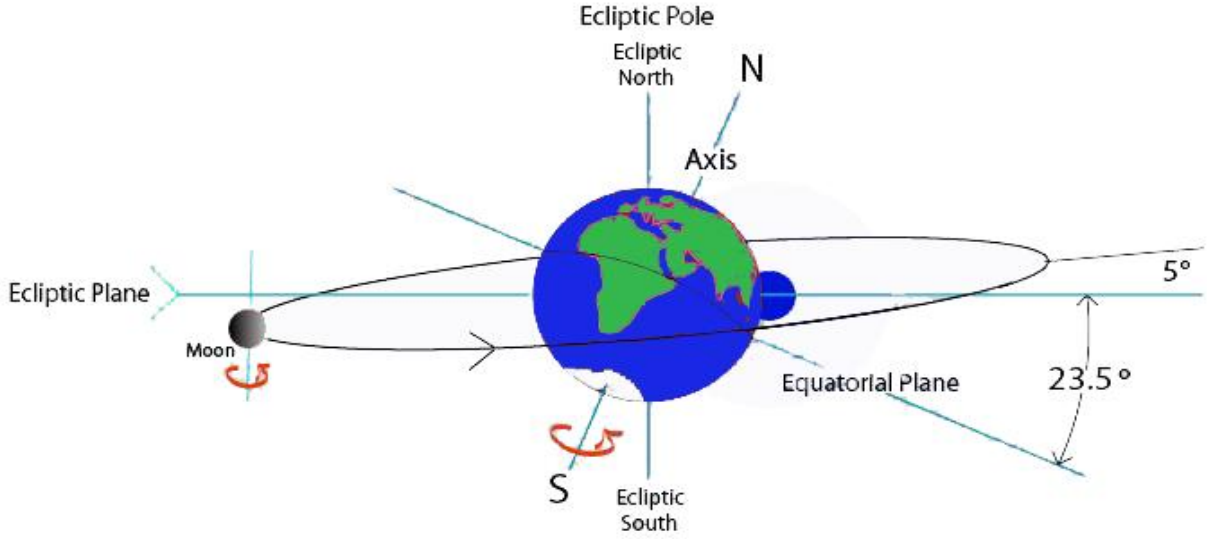

Figure 11. The true NCP is inclined at 23.5^{o} from the ecliptic pole and coincides with the Earth's axis of rotation.

A rough alignment can be achieved by pointing the telescope at the North Star which is ¾ of a degree off the true NCP. Further alignment instructions are given in the CG-5 mount instruction manual. Any drift of the moon out of the scope's field of view may be a result of inaccurate alignment and can be eliminated to a great extent by the declination drift method (see CG-5 manual).

3.3. Spectral retrieval and processing

The spectral range for the spectrometer was calibrated from 550-850 nm. Each spectrum processed must be an average of several thousand individual spectra. Averaging of 3000 to 6000 spectra was used to improve the signal to noise ratio.

Depending on the light intensity from the Moon, integration times from 100 ms to 250 ms were chosen such that the intensity (counts) axis does not reach saturation. Integration times above 250 ms are not desirable since this indicates too little light intensity. For example using an integration time of 500 ms with 6000 averages as a target would require 3000 s (50 min). A single data point obtained over 50 min interval would carry little information on how absorbers are distributed in more narrow timeframe. A typical Moon (550-850 nm) spectrum obtained during our campaign is illustrated on Fig. 12 below.

For the analysis of an absorber, one must use a laboratory measured cross section of that absorber . The spectrum of NO_3 is illustrated on Fig. 13. Then the laboratory measured reference cross section must be "convoluted" with the slit function of the spectrometer, by applying the method of least squares (Platt, 2008; pp. 292-295). For this purpose, a very fine emission line is used, typically obtained by measuring a mercury lamp spectrum (Fig. 14). Also, one must account for other absorbers that share features in the wavelength region of NO_3.

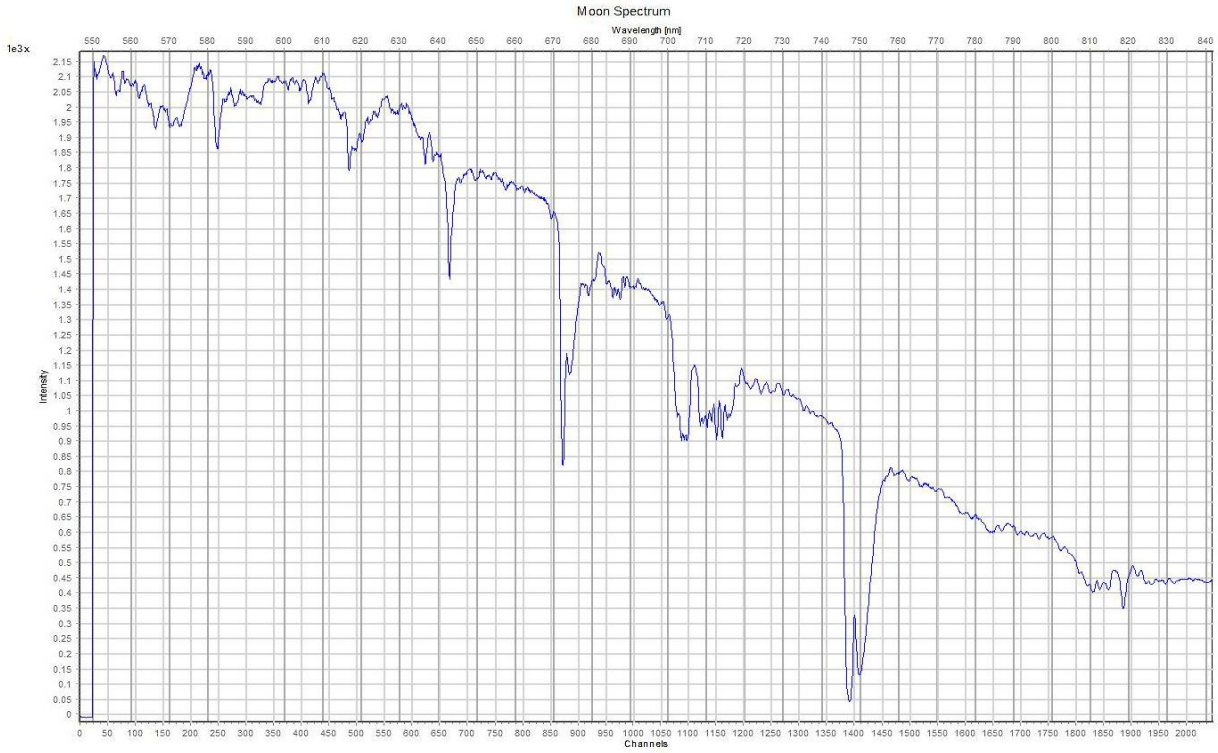

Figure 12. Moon spectrum. 31.03.10; 5:25 AM; 6000 averages; 150 ms

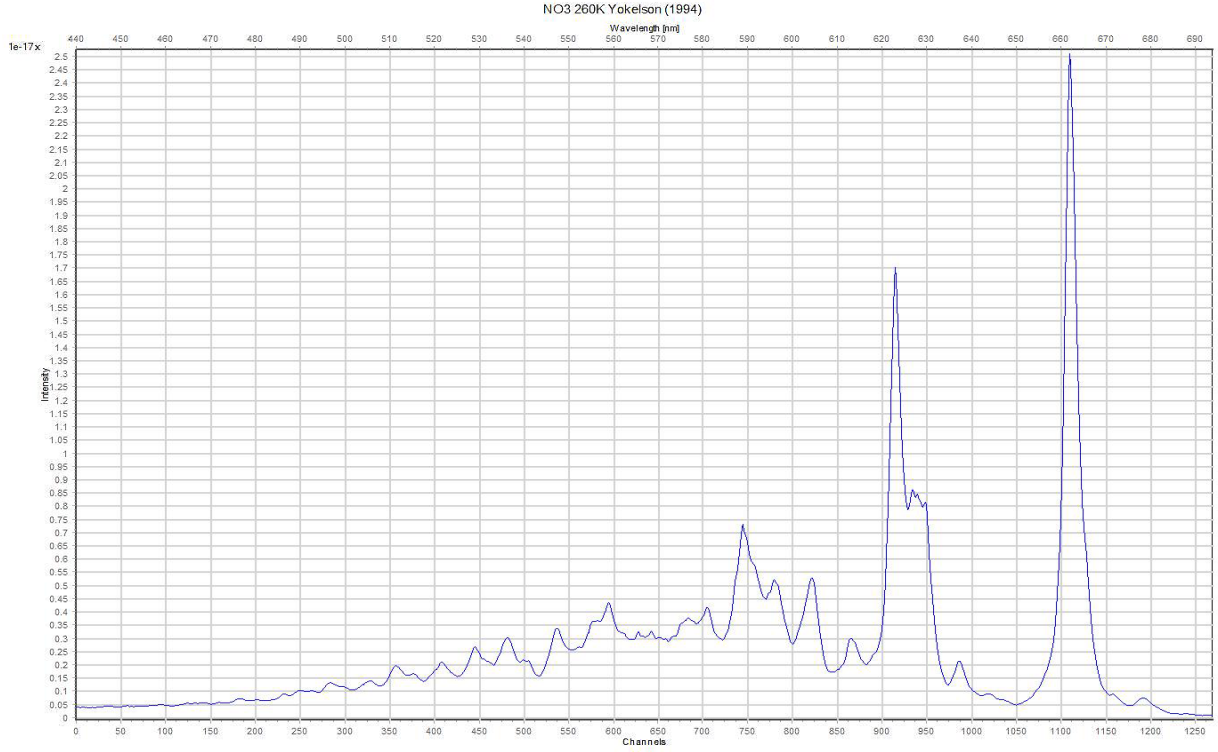

Figure 13. NO_3 laboratory measured absorption cross section as measured by Yokelson (1994) at 260K with major strong absorption features near 625 nm and 662 nm

Fraunhofer reference spectrum and ring spectrum need to be applied to a fit scenario for the complete analysis of the trace absorber. Discussion of these follows below. Absorption spectra always contain noise that needs to be removed because it carries statistical uncertainty. The dark noise therefore must be subtracted from the original spectrum.

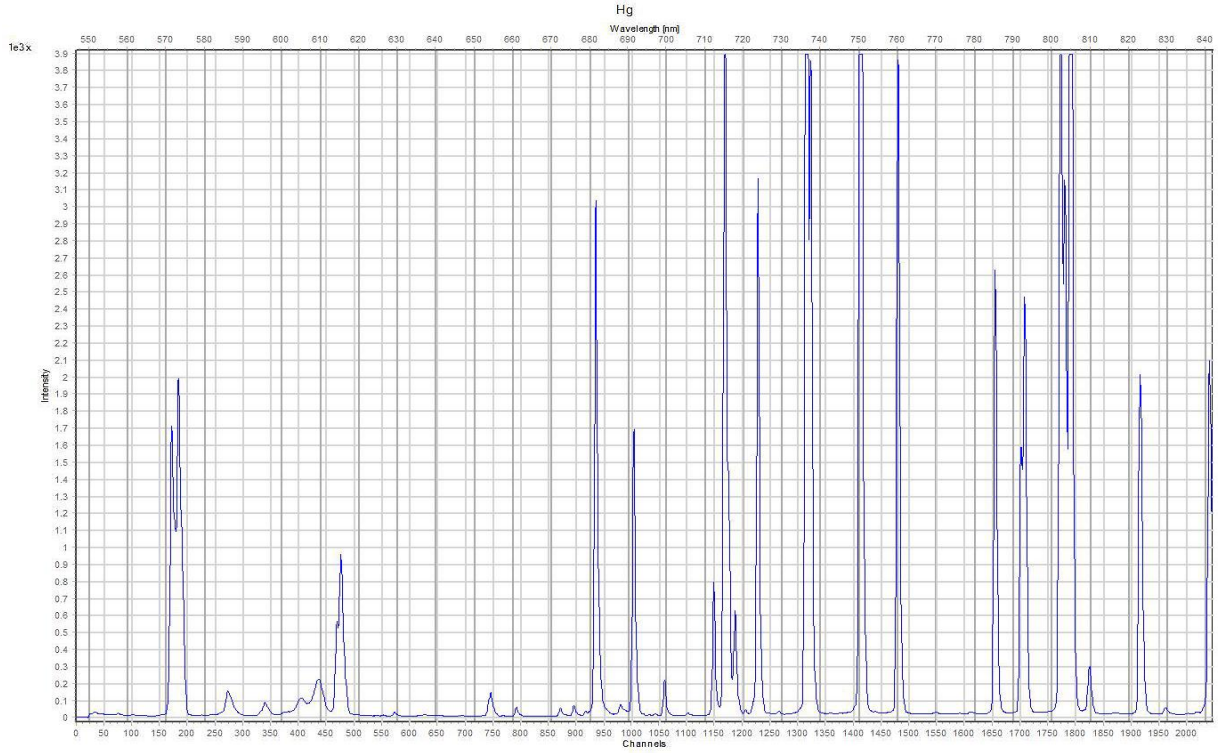

Figure 14. Mercury (Hg) lamp spectrum. A single line must be used for the convolution.

An example of a fit result for 658-668 nm is illustrated on Fig. 15. It is important that the reference spectra are well aligned with the reference absorption spectrum. However, small uncertainties may arise in the wavelength position and dispersion due to thermal changes in the spectrometer. This is why it is important that the spectrometer is kept at a constant temperature, to the nearest tenth of a degree, throughout the whole campaign so that dark current is minimized. Also due to inaccuracy with wavelength calibration by the Hg spectrum, and errors of literature absorption cross sections, it is important that a few parameters are corrected for the final fit result. One parameter allows wavelength shift for a theoretical fit and must be at

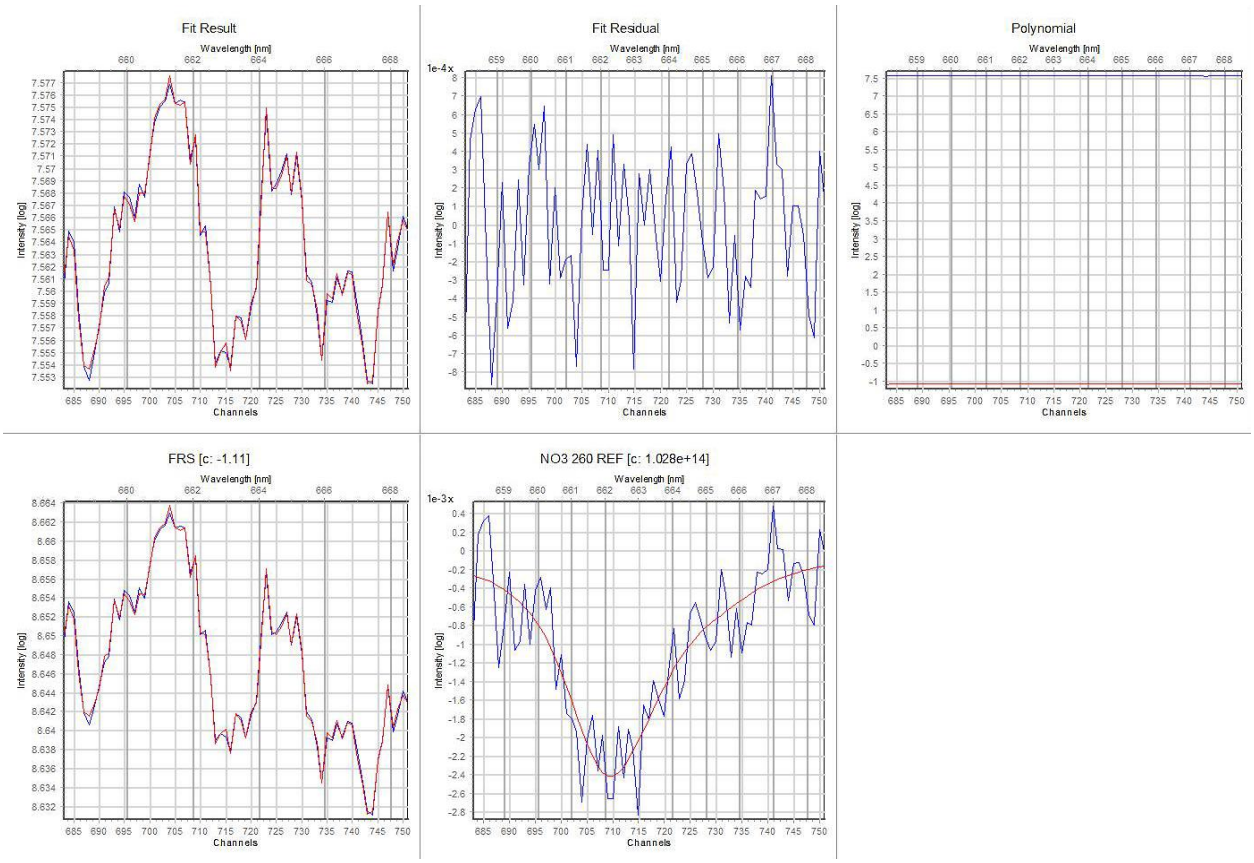

Figure 15. DOASIS NO_3 fit example. Shift ±0.2 nm; squeeze: 0.999-1.001 nm. NO_3 has a major absorption feature seen at 662 nm. The fit residual is low which means that the fit is very good.

maximum ±0.2 nm. The other parameter involves squeezing. If not constrained, this parameter may affect the true concentration and introduce unwanted structures in the fit residual (Platt, 2008; p. 298). For optimal results, squeeze should be in a range of 0.999-1.001 nm. The whole fit procedure used by DOASIS can be seen mathematically in the following way:

$$\ln I = \ln I_o - \sigma S - polynomial \tag{14}$$

where S is the fit result or the SCD. Thus the left side of the equation is our measured spectrum and the right side is the spectrum that contains the absorber. The difference is the fit residual which must be as small as possible so that the equation holds true, i.e. the fit is good.

4. Results and Discussion

Measurements of NO_3 vertical columns were carried in a mid-latitude location, using direct moon light throughout the winter of 2009/10 on the William Small parking roof at York University (43^o 46' N - 79^o 30' W; 199 m a.s.l.).

4.1 The instrument

Equatorial mount alignment difficulties were encountered on various occasions throughout the campaign. For this reason, as well as local weather and lunar constraints we were able to collect data for the nights of 04/05, 05/06, 29/30 and 30/31.03.2010 for the period of Nov 2009 – Mar 2010. The data acquisition was optimal for ~80 to 100% illuminated moon (Fig. 16). This would allow for exposures of about 4 days before full moon (Waxing Gibbous) and about 4 days after (Waning Gibbous). A comprehensive moon data is given below (Table 2). The most

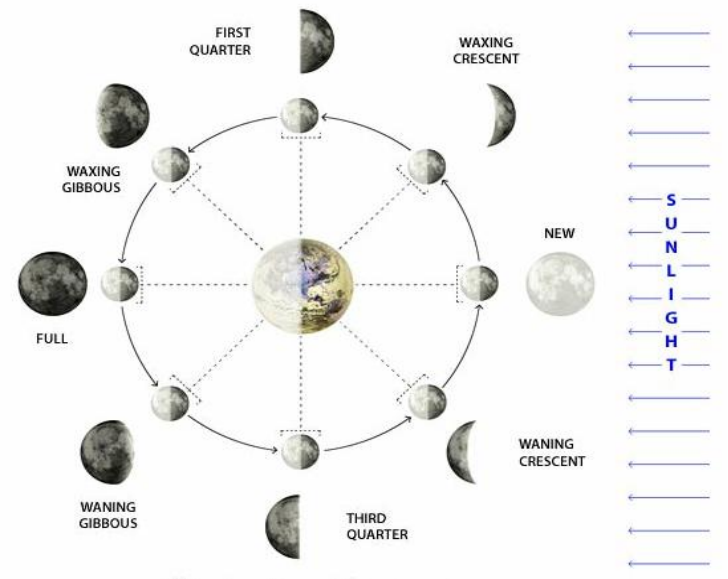

Figure 16. Moon phases. Maximum light intensity was utilizable by DIM-DOAS on days including phases from Waxing Gibbous (~80) to Waning Gibbous(~80).

sensitive measurements were possible towards the end of Mar 2010 when the image of the Moon was sufficiently bright and (LZA range was from about 55^o to 80^o) not obscured by clouds.

Table 2: Moon statistics

Date	Moonrise	Moonset	LZA(degree)	Distance (km)	Illuminated (%)	Phase
Mar 4 2010	23:37	08:24	max 90-61 min	374310	82.1	
Mar 5 2010	00:00	08:59	max 90-65.1 min	380850	72.7	
Mar 29 2010	19:38	06:24	max 90-56.2 min	362629	98.6	Full at 22:25
Mar 30 2010	20:56	06:51	max 90-52.6 min	365062	99.8	

4.2 Spectral analysis

We have treated the acquired data in a way similar to previous studies (Aliwell and Jones, 1996, 1998; Wagner et al., 2000). From the absorbers that share features in the 550 – 850 nm range, we only considered NO_3 and H_2O, since O_3 shows broadband structure, and O_4 as well as NO_2 do not have strong absorption features anywhere near the 662 nm NO_3 band. Convoluted, laboratory measured cross sections of NO_2, O_4 and H_2O are shown below (Fig. 17, 18, 19). A temperature dependent NO_3 cross section (Yokelson et al. 1994) of NO_3 measured at 260K was used for the fit, similar to other studies (Wagner et al., 1998; 2000).

Although the exact correction of the H_2O absorption is a prerequisite for the correct NO_3 evaluation, studies (Wagner et al., 2000) have shown that H_2O absorption near 650 nm has very small influence on the retrieved NO_3 slant column concentrations. Therefore, we have chosen not to fit H_2O, since the analysis where H_2O is included can be complicated due to the fact that the atmospheric temperatures where H_2O absorbs could have been substantially different than the temperature at which the H_2O cross-section was retrieved. This would require fitting of different

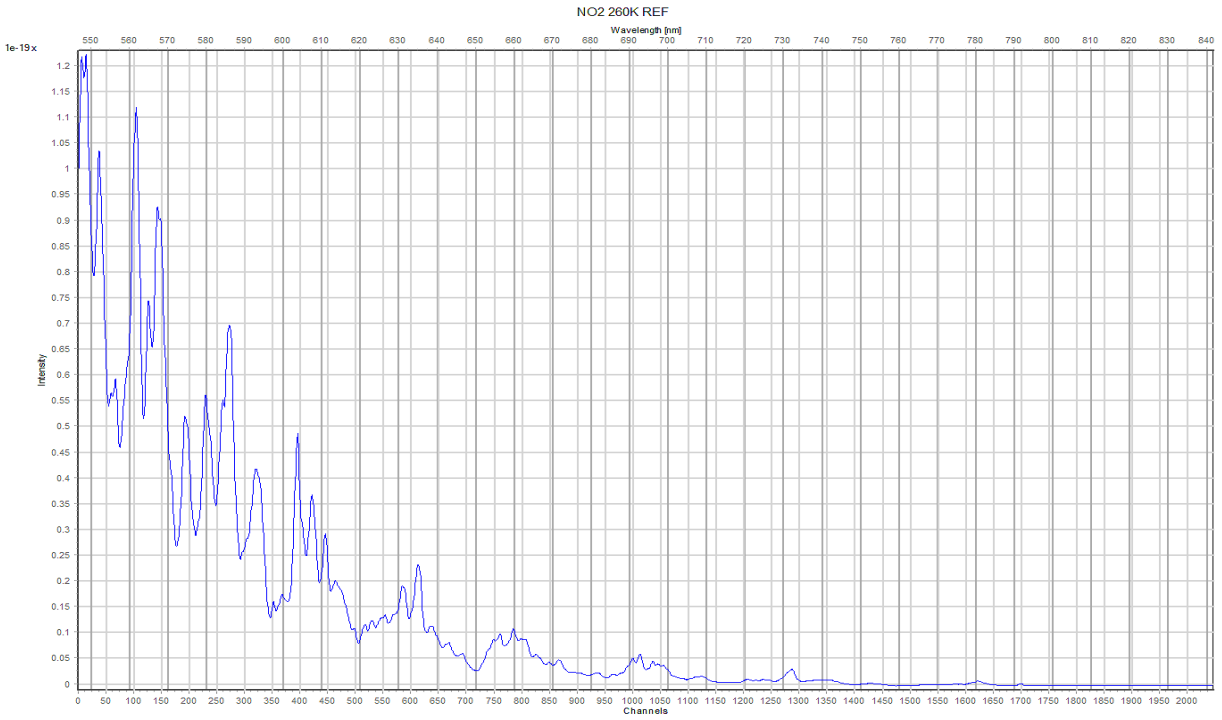

Figure 17. Convoluted NO_2 cross section (Voight, 2002). NO_2 absorption cross section shows very weak absorption feature near 662 nm.

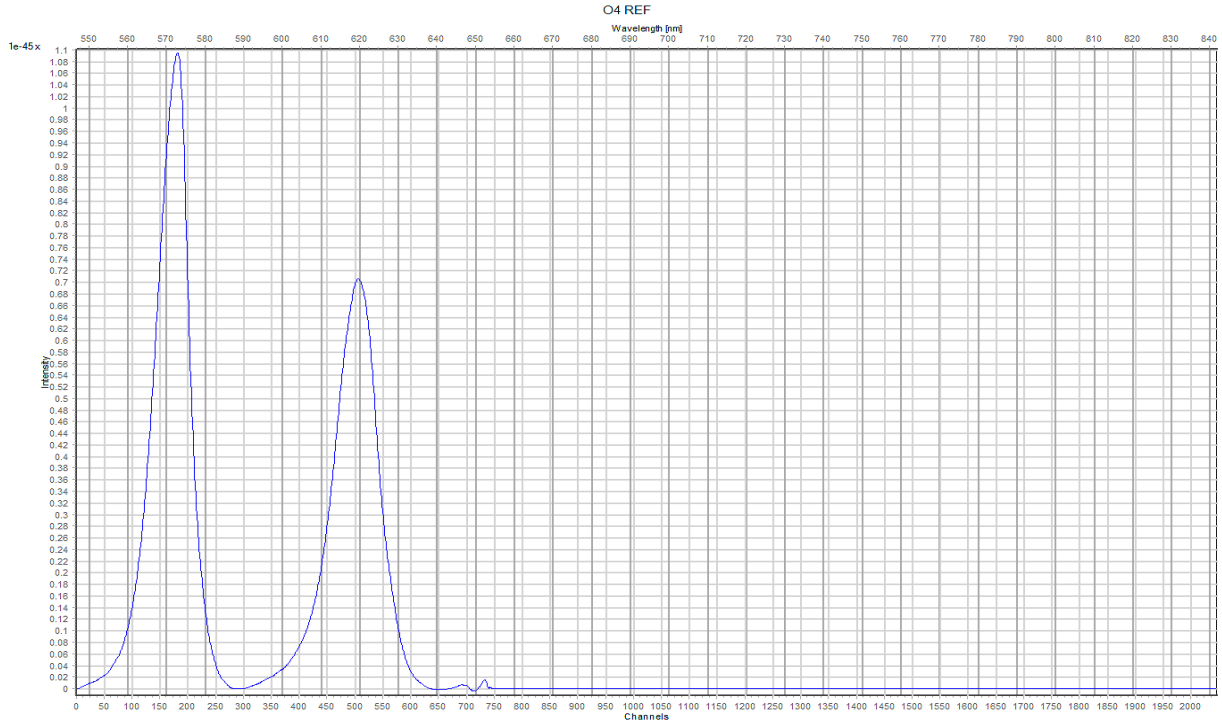

Figure 18. Convoluted O_4 cross section (Hermans). O_4 absorption in the range of 550 – 850 nm shown no features near 662 nm.

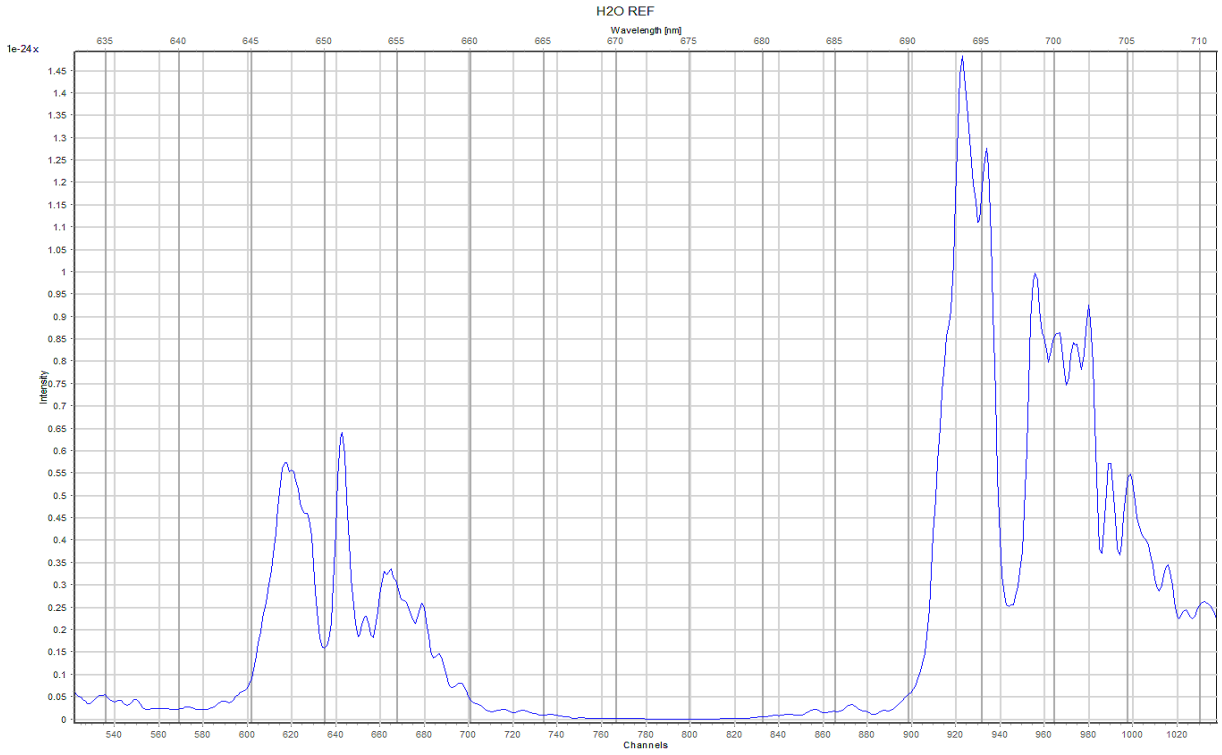

Figure 19. Convoluted water vapour absorption cross section. Water has a weak absorption feature near 658 nm with no significant influence on NO_3 662 band absorption.

temperature cross sections of H_2O. Therefore we only fit NO_3 in a narrow 10 nm (658-668 nm) region as it is shown for 30/31.03.2010 below (Fig. 20). This fit ensured the proper removal of Rayleigh scattering and Mie scattering but had no account for H_2O absorption . Nevertheless the fit was considered good since no major features were observed in the very low residual spectrum as can be seen in the top middle panel of Fig. 20. Results for DSCDs of NO_3 obtained this way would contain the error of the uncertainties of the fit procedure and the determination of the cross sections (±4.5% for Yokelson's NO_3 cross section). However the error for the VCDs was attributed to a combination of other factors discussed later.

The reference spectrum used for the fit was measured at ~80^o LZA (6:07 AM on 06.03.2010) when the SZA was ~95^o and it was expected to have low concentration of NO_3 since

by that time NO_3 would partly photolyze to due to the progress of the solar terminator through the atmosphere (Smith and Solomon, 1990, 1993).

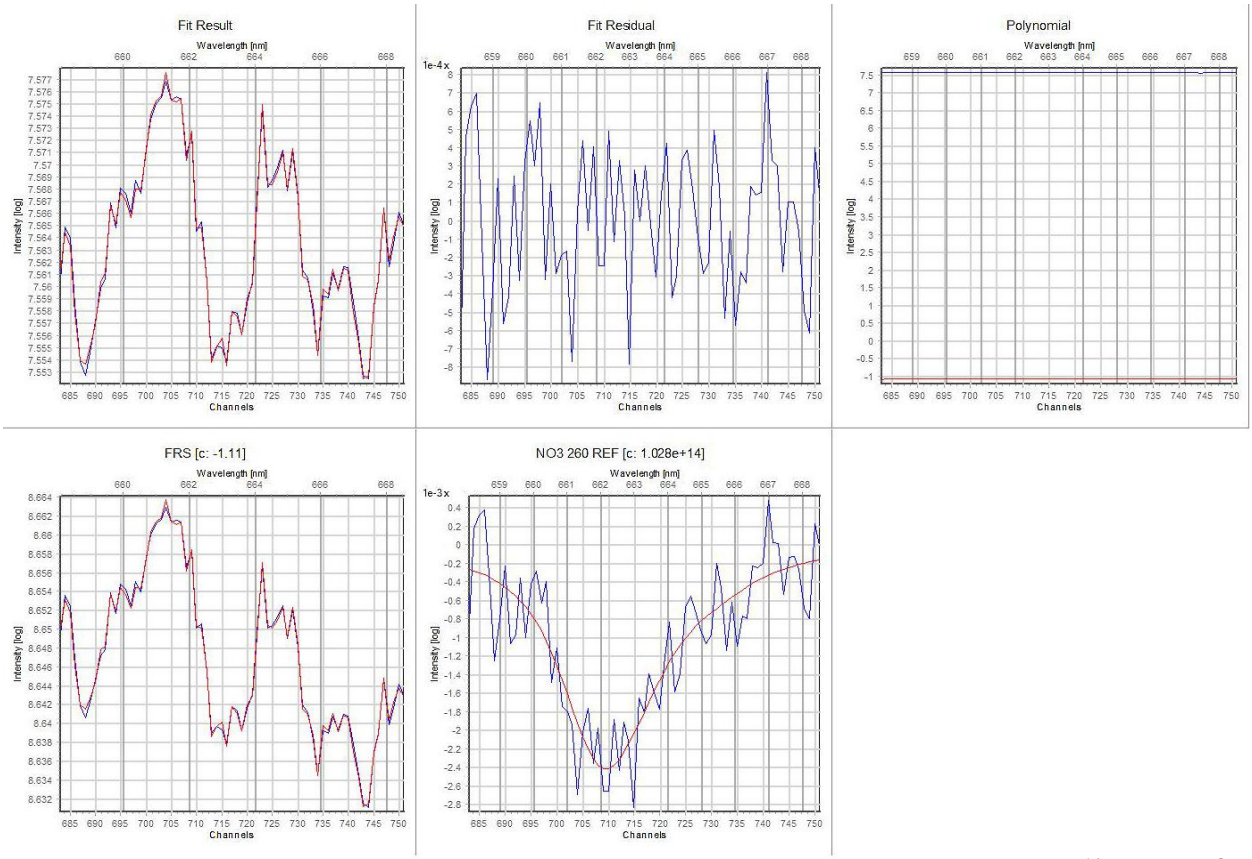

Figure 20. DOASIS fit result for NO_3 on the morning of 31.03.10, 5:56 AM. NO_3 DSCD is $1.028 \cdot 10^{14}$ molec cm^{-2}. The red curve represents the laboratory measured cross section of NO_3 (Yokelson et al., 1994) at 260K. The blue curve is the one measured by DIM-DOAS, Ocean Optics S2000 spectrometer.

4.3 Calculation of the vertical columns

The DSCDs obtained by the fit analysis did not represent the absolute concentrations. As mentioned already, to remove the strong Fraunhofer structures, each spectrum was divided by a reference spectrum taken at a low LZA. Because the LZA was approximately 80^o when the reference was retrieved and the SZA was ~95^o, we estimated that the reference spectrum must contain some NO_3. Therefore the result from the DOAS analysis represents the difference of the slant column density of the measured spectrum measured at zenith angle θ and that of the

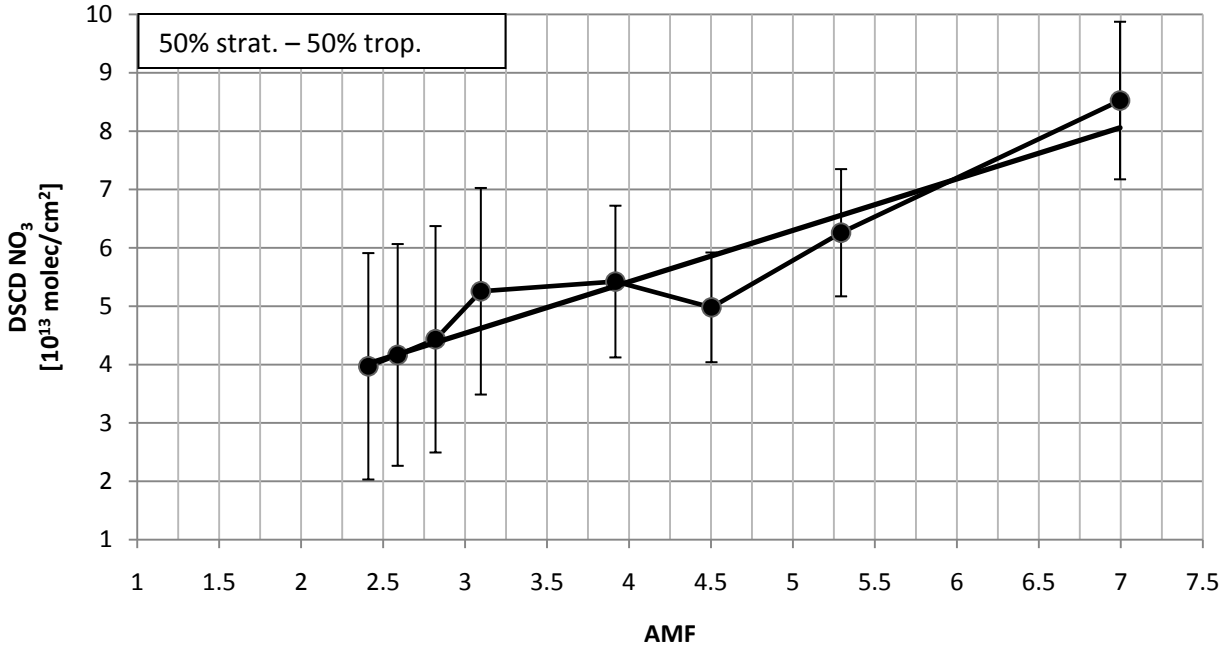

Figure 21. Langley plot for 29/30.03.2010. As the LZA increases, the AMF approaches a value of ~40 at 88^{o} angle. At the horizon (LZA = 90^{o}), the AMF is an infinitely large number.

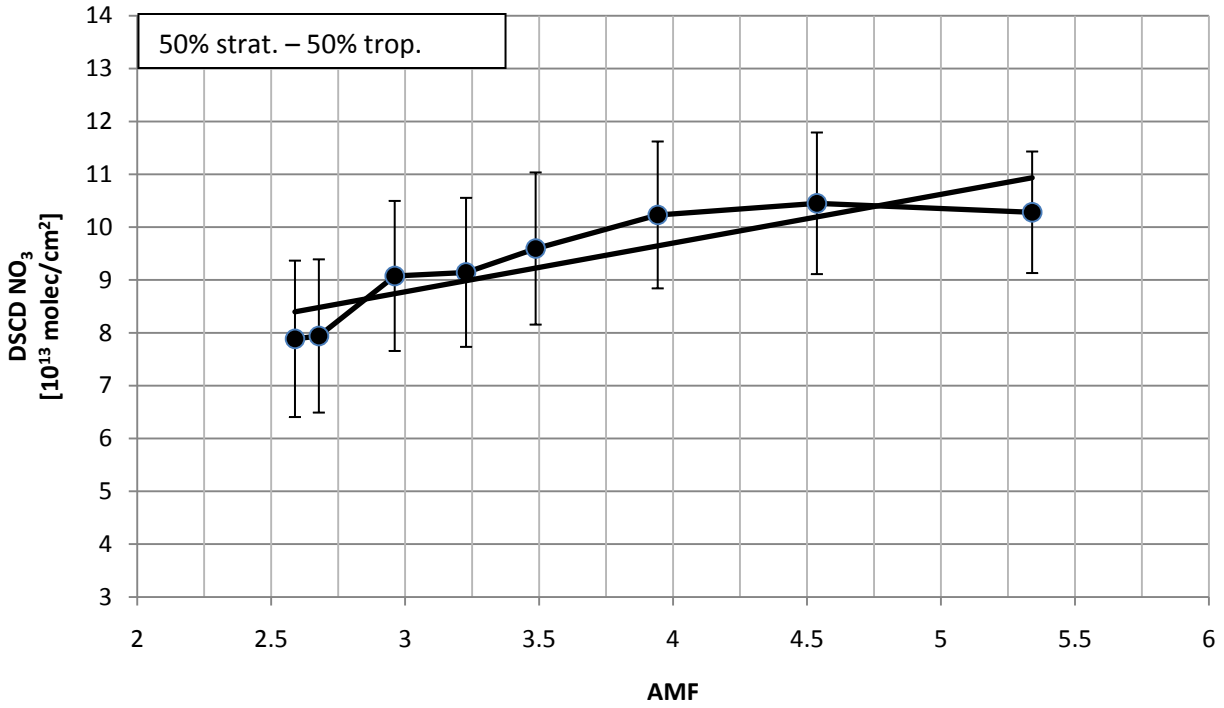

Figure 22. Langley plot for 30/31.03.2010. The plot shows variation from night to night due to difference in atmospheric composition.

reference spectrum, measured at zenith angle θ_{ref}. In order to estimate how much NO_3 was present in the reference spectrum, we constructed Langley plots (Fig. 21 and 22) that show the variation of NO_3 DSCDs with AMF. The measured $DSCD_m$ was given by:

$$DSCD_m = DSCD_{diff} - DSCD_{ref} \tag{15}$$

where:

$$\begin{aligned} DSCD_{ref} &= VCD_{ref} AMF_{ref} \\ DSCD_{diff} &= VCD_{diff} AMF_{diff} \end{aligned} \tag{16}$$

and:

$$DSCD_m = VCD_{diff} AMF_{diff} - VCD_{ref} AMF_{ref} \tag{17}$$

After substituting (15) into (8), the absolute VCD was calculated according to:

$$VCD = \frac{DSCD_{diff}}{AMF} = \frac{(DSCD_m + DSCD_{ref})}{AMF} \tag{18}$$

The slope of the Langley plot was determined as the VCD_{ref}. This concentration was constant and was added to the VCD_m calculated from the fit.

Langley plots were constructed for purely stratospheric scenario, using 1/cos(LZA) and for purely tropospheric scenario, using 1/sin(EA). Since the plots showed identical it assumed that they represent a mixed 50% stratospheric and 50% tropospheric profiles. Recent report (Wagner et al., 2000) estimated that in the Antarctic winter the NO_3 atmospheric profiles are also mixed with 75% of the NO_3 column in the stratosphere. Langley plots for the nights of 04/05 and 05/06.03.2010 were not constructed since data was collected for shorter times. It was therefore expected that the reported for these nights vertical columns were higher.

4.4. Results

From the Langley plots for 29/30 and 30/31.03.2010, the NO_3 $DSCD_{ref}$ were determined as $1.9\pm0.2\cdot10^{13}$ molec cm^{-2} and $2.0\pm0.4\cdot10^{13}$ molec cm^{-2}, respectively. The estimated error includes the error associated with the nocturnal variations of NO_3. These results were added to the measured DSCDs to give an average of $5.7\cdot10^{13}$ molec cm^{-2} and $7.8\cdot10^{13}$ molec cm^{-2} for the nights of 29/30.03.2010 and 30/31.03.2010, respectively. We also correlated the NO_3 slant columns with the lunar zenith angle and as expected, higher concentrations were seen for higher LZAs, and lower concentrations for lower LZAs. The correlations are illustrated on Fig. 23 and 24 for the nights of 29/30.03.2010 and 30/31.03.2010, respectively.

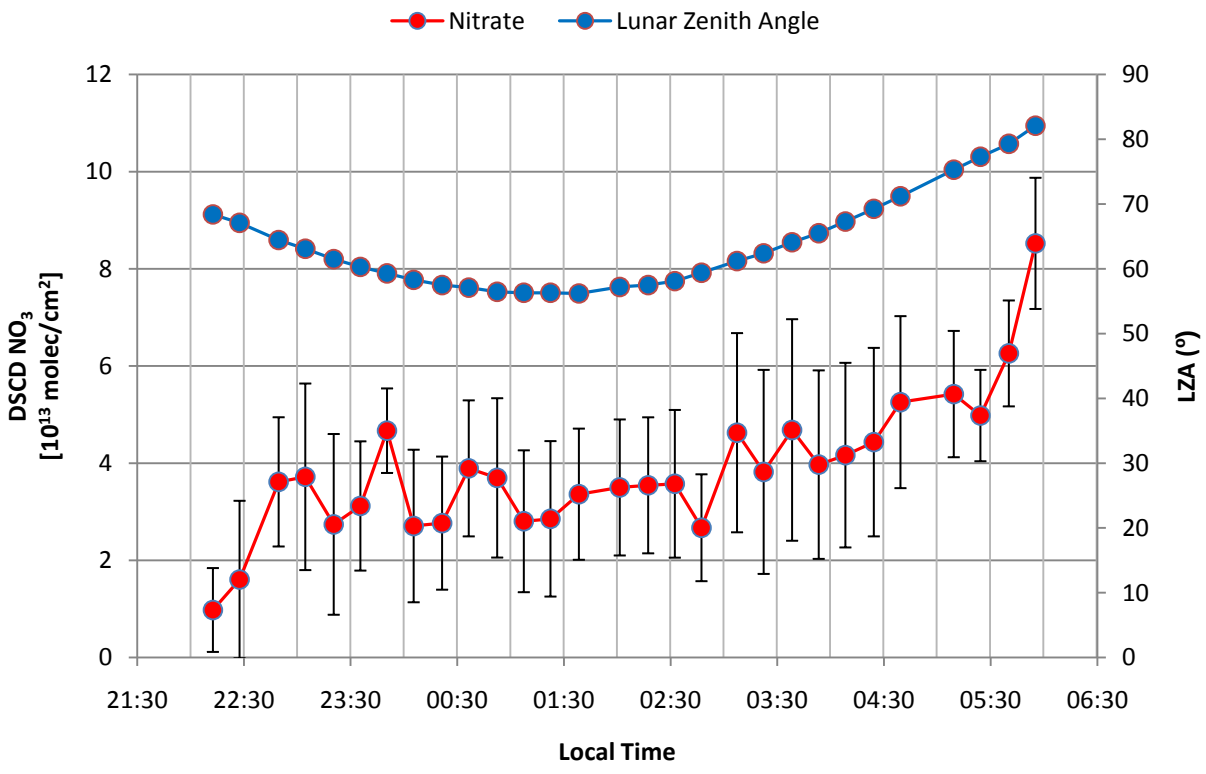

Figure 23. Correlation of LZA with the measured DSCD of NO_3 for 29/30.03.2010

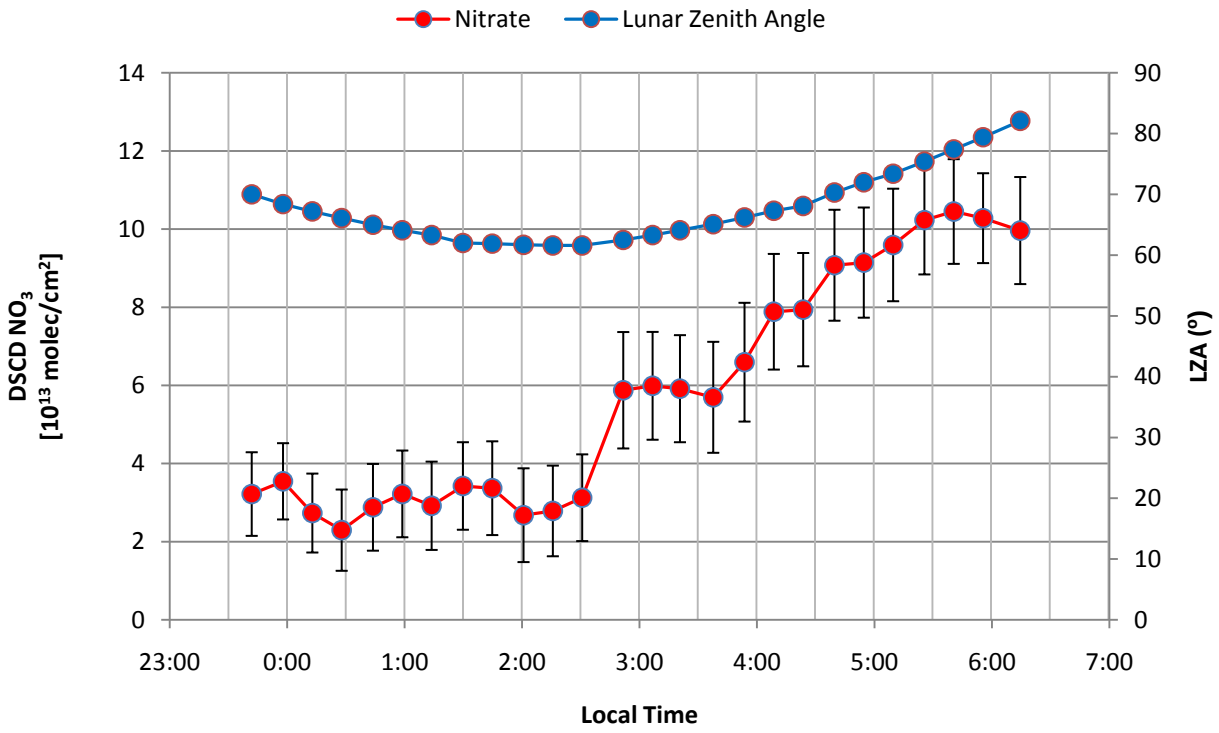

Figure 24. Correlation of LZA with the measured DSCD of NO_3 for 30/31.03.2010

In the late 80s DSCD abundances of NO_3 have been reported as $2 \cdot 10^{13}$ molec cm^{-2} (Sanders et al., 1987) at 78°S by monitoring the spectral interval of 640-670 nm. Another study reported much higher average DSCDs of $2.1 \cdot 10^{14}$ molec cm^{-2} above Cambridge, England (Weaver et al., 1996). Preliminary calculations based on recent reports (Brown at al., 2007) suggested that above 300 m altitude there must be a strong gradient of NO_3. Considerations based on kinetic data (JPL, 1997) suggested that NO_3 DSCD is as high as $1 \cdot 10^{13}$ molec cm^{-2} above 300 m or even higher. The DSCDs we measured, confirmed the preliminary expectations and made a good agreement with the literature.

Our measurements from 29/30.03.2010 (Fig. 25) and 30/31.03.2010 (Fig. 26) showed NO_3 VCDs of $2.8 \cdot 10^{13}$ molec cm^{-2} and $3.6 \cdot 10^{13}$ molec cm^{-2}, respectively. For the night of 29/30.03.2010 the VCD remain almost unchanged with average of $3 \cdot 10^{13}$ molec cm^{-2}. Maximal

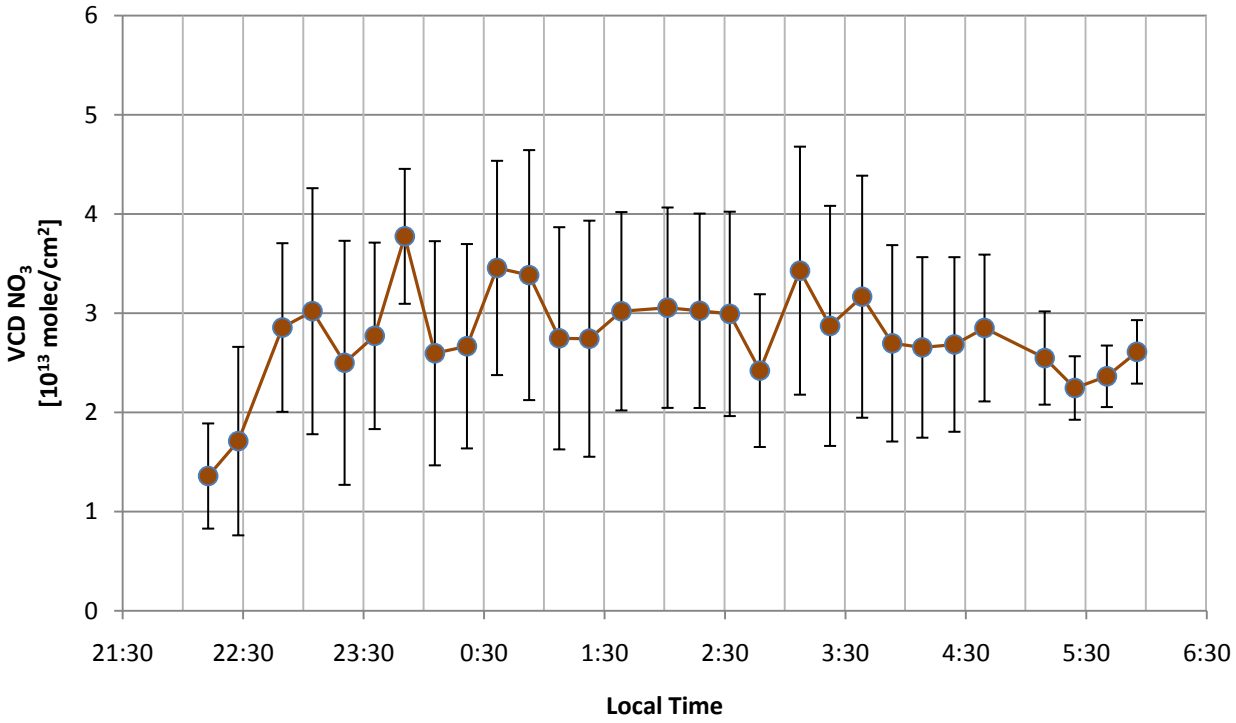

Figure 25. Vertical column density of NO_3 for 29/30.03.2010. No variation in the VCD was seen for the night.

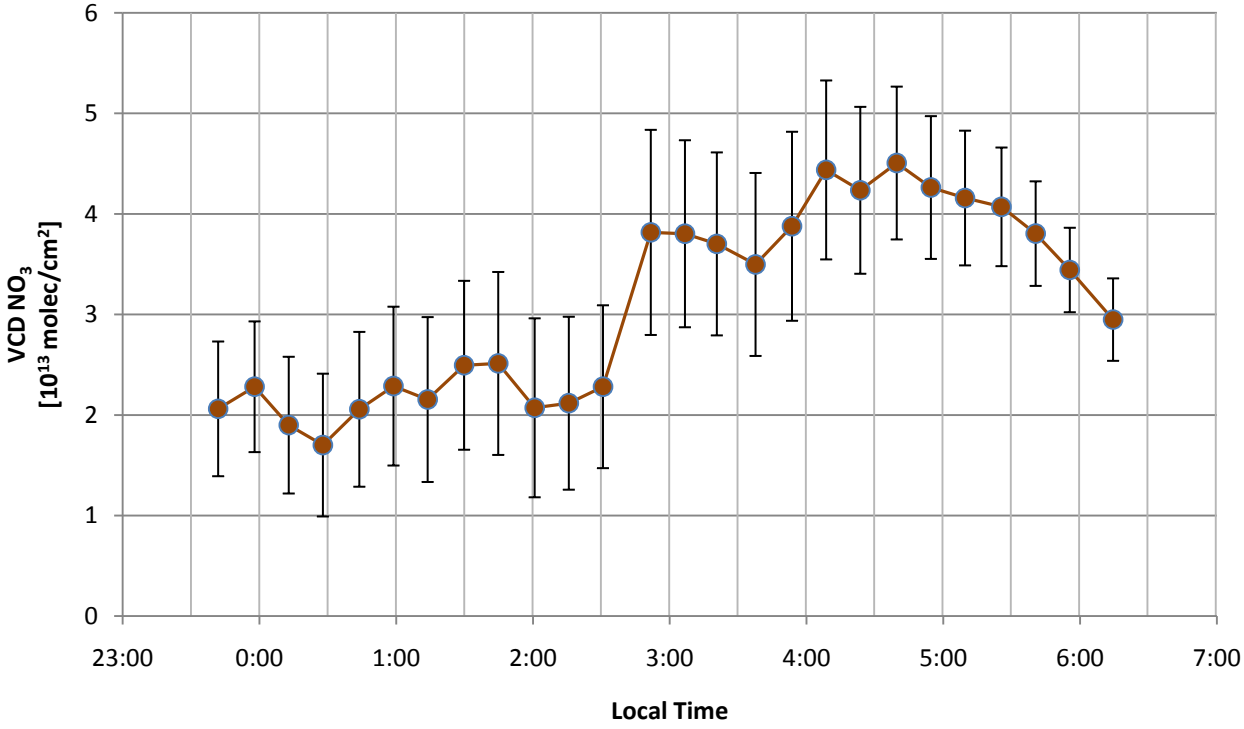

Figure 26. Vertical column density of NO_3 for 30/31.03.2010. The VCD of NO_3 doubled after 3:00 AM in the morning of 31.03.10

concentration of $3.8 \cdot 10^{13}$ molec cm^{-2} was established at midnight for the same night. Significant variation of the VCD was observed on the next night (30/31.03.2010). For the first three hours of that night the column was an average of $2 \cdot 10^{13}$ molec cm^{-2} but doubled in concentration at 3 AM on the morning of 31.03.2010. A maximum concentration of $4.5 \cdot 10^{13}$ molec cm^{-2} was reported at 4:40 AM.

Stratospheric NO_3 concentrations exhibit relatively steady concentrations, given that transport in the stratosphere is slow and would not trigger significant changes in the NO_3 concentrations. From the Langley plots, it was previously discussed that the column of NO_3 is of mixed stratospheric and troposheric character. To understand what triggered the variation in the VCD, we looked at O_3 data (Fig. 27) retrieved for the same night by a TECO instrument from our laboratory, as well as meteorological data (Fig. 28) from the York university ESSE station.

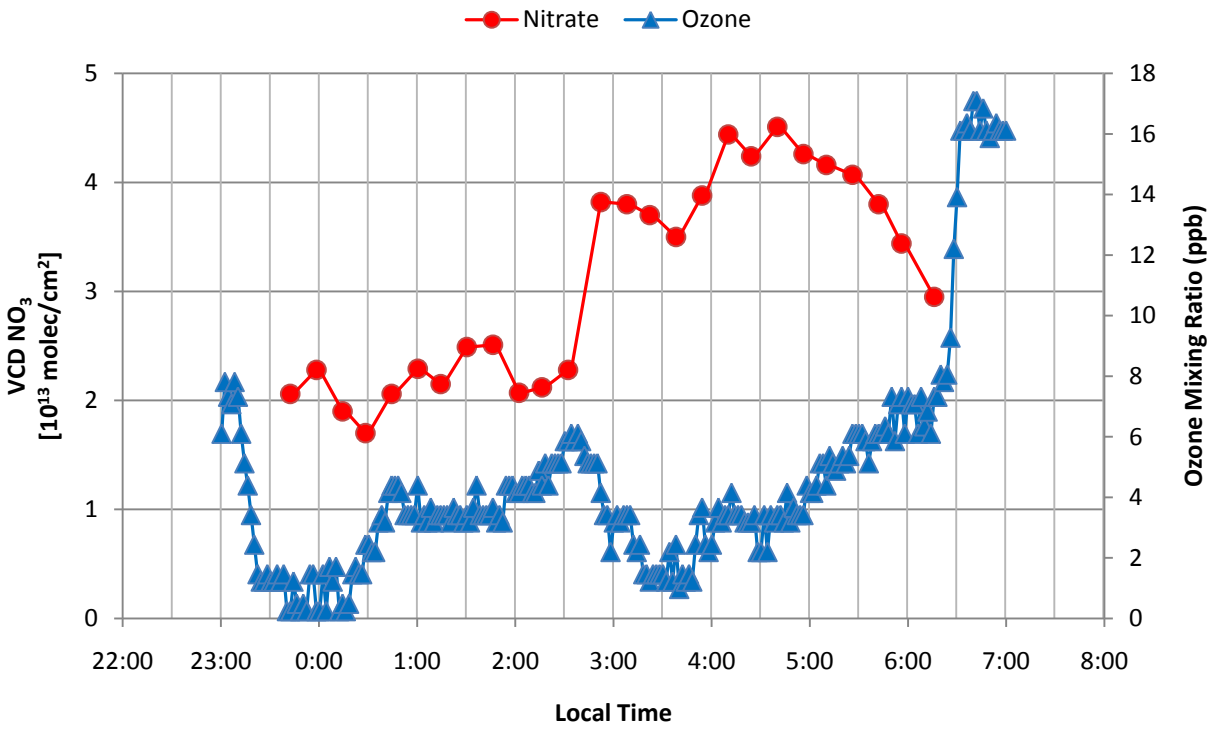

Figure 27. Correlation of the measured NO_3 VCD with O_3 for 30/31.03.2010

The relatively steady VCD from 11:30 PM on the 30.03 to 2:30 AM on 31.03 was attributed to the stratosphere since no significant change was expected there. Therefore the increase at 3:00 AM was owing to some event in the troposphere. To support this argument, from Fig. 27 it is apparent that O_3 reduction from ~6 ppb to 1 ppb takes place at the instance when the VCD of NO_3 increased. In principle this could be a titration reaction of NO with O_3 to give NO_2. Since O_3 did not reach zero concentration, it may have reacted further with NO_2 to give NO_3 in the troposphere.

According to Air Quality Ontario, North Toronto station, there was an increase of NO_2 by 6-7 ppb on the morning of 31.03.10 (Fig. 29). Therefore we expected that NO_2 was either transported in a local plume, observed that same morning, or it built up locally. The wind profile retrieved from York university ESSE meteorological observation station did not show an evidence of transport. The only possibility left open was that NO_2 was built up locally.

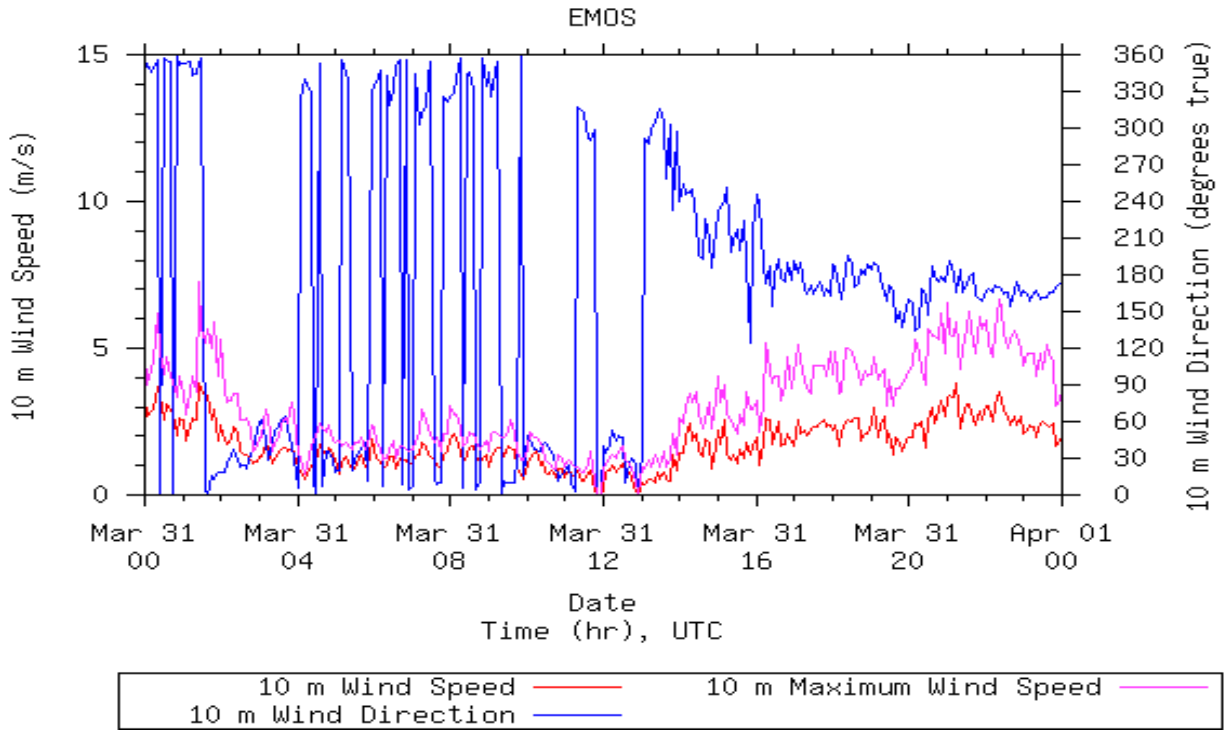

Figure 28. Wind profile for of 30/31.03.10 measured by York ESSE meteorological station. Local time is UTC - 4h.

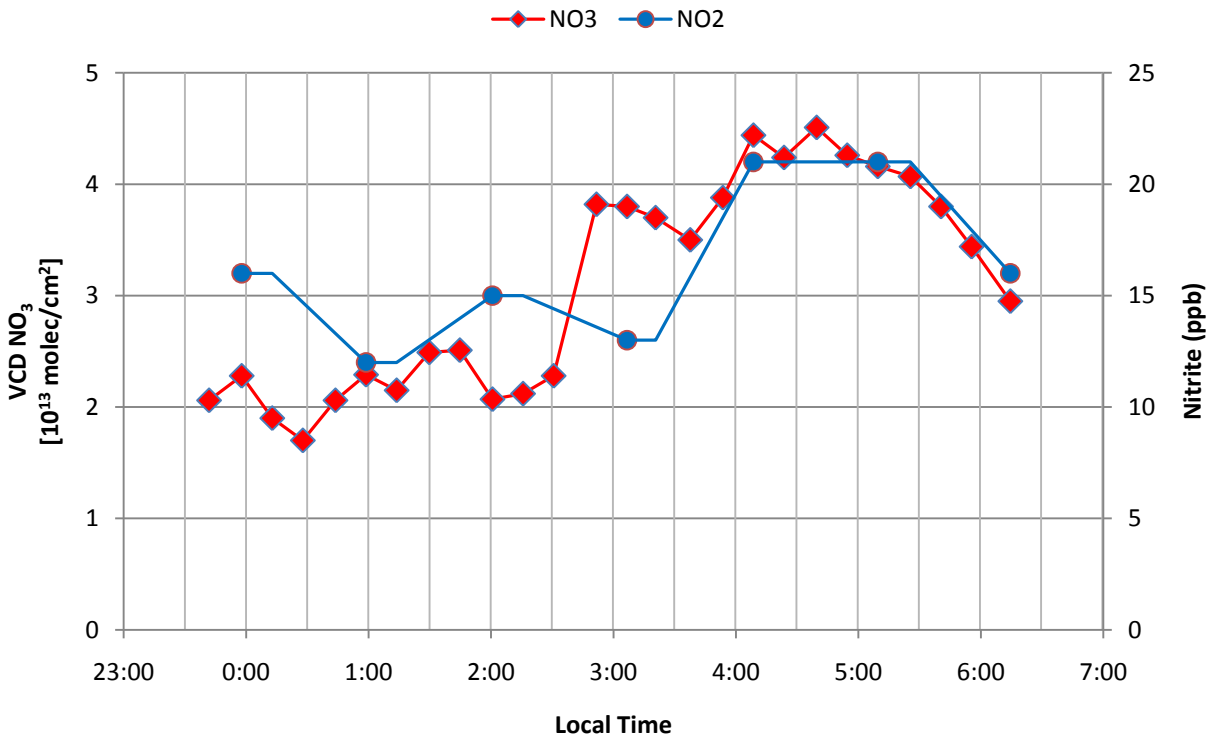

Figure 29. Correlation of the measured NO_3 VCD with NO_2 for 30/31.03.2010. The NO_2 mixing ratio is measured by Air Quality Ontario, North Toronto station.

Given this interpretation we attributed the increase of the NO_3 VCD to a stratospheric phenomenon for the morning of 31.03.2010.

A summary for the whole campaign (Nov 2009 – Mar 2010) is presented in Table 3. The error associated with the VCDs of all measurements was associated with the uncertainty in the laboratory measurements of the NO_3 cross section, the fit, as well as the $DSCD_{ref}$ obtained from the Langley plots and the calculation of the AMF. The VCD were not determined for 04/05.03.2010 and 05/06.03.2010 because the $DSCD_{ref}$ was not determined for these nights.

Table 3: Summary of NO_3 slant columns and vertical columns for the winter 2009/10 . *VCDs were not calculatd since $DSCD_{ref}$ was not determined

Date	NO_3 DSCD (10^{13} molec cm^{-2})	NO_3 VCD (10^{13} molec cm^{-2})
04/05.03.2010	1.19±0.36	*
05/06.03.2010	2.60±1.17	*
29/30.03.2010	5.73±1.77	2.77±0.92
30/31.03.2010	7.80±1.26	3.60±0.82

5. Conclusions and future work

The study successfully implemented a system for measurement of NO_3 VCD using direct moon light DOAS. The VCDs were in the range of $1\text{-}4\cdot10^{13}$ molec cm^{-2}, similar to the range seen in other studies of urban areas. The study also brought an insight as to how NO_3 was distributed in the stratosphere and the troposphere in urban areas.

An increase in the NO_3 VCD was seen in one night after there was an evidence of an increase in air pollution in the troposphere. Therefore it was suspected that the increase of NO_3 VCD by $\sim2\cdot10^{13}$ molec cm^{-2} was due to tropospheric pollution.

Further work would require that the NO_3 fit include H_2O absorption spectrum in order to see how it would influences the DSCD of NO_3. This will provide more accurate determination of the absolute DSCDs. Yet, another important aspect is to fit NO_2 in the acquired data. This can be very informative as to how NO_3 behaves depending on NO_2 concentrations.

Future work will extend the study to simultaneous direct moonlight and ground-based measurements in order to create profiles that will better explain the NO_3 vertical distributions. A study of this type can provide important evidence on tropospheric pollution, that remained inconclusive in this study.

Summer time measurements in urban areas will be anticipated.

References

1. Aliwell, S. and Jones, R.: Measurements of atmospheric NO_3. Improved removal of water vapour absorption features in the analysis for NO_3, *Geophys. Res. Lett.* 23 (**1993**), 2585-2588

2. Aliwell, S. and Jones, R.: Measurements of troposheric NO_3 at midlatitude, *Geophys. Res. Lett.* 103 (**1998**), 5719-5727

3. Brandenburger, U., Brauers, P., Dorn and H.-P., Hausman, M.: In-situ measurements of tropospheric hydroxyl radicals by folded long path lasers absorption during the field campaign POPCORN in 1994, *J. Atmos. Chem.* 31 (**1998**), 181-204

4. Brown, S., et.al.: High resolution vertical distribution of NO_3 and N_2O_5 through the nocturnal boundary layer, *Atmos. Chem. Phys.* 7 (**2007**), 139-149

5. Fowler, D., et al.: Atmospheric composition change: Ecosystems - Atmosphere interactions, *Atmos. Env. 43* (**2009**), 5193-5267

6. Honninger, G., Friedeburg., C. and Platt, U.: Multi axis differential optical absorption spectroscopy (MAX-DOAS), *Atmos. Chem. Phys.* 4 (**2004**), 231-254

7. Demore, W. and Sander, S.: Chemical kinetics and photochemical data for use in stratospheric modeling, *Jet Prop. Lab.* 97-4 (**1997**), 263

8. McLaren, R., Salmon, R., Liggio, J., Hayden, K., Anlauf, K. and Leaitch, W.: Night time chemistry at the rural site in the Lower Fraser Valley, *Atmos. Env.* 38 (**2004**), 5837-5848.

9. McLaren, R., Wojtal, P., Majonis, D., McCourt, J., Halla, J. and Brook, J.: NO_3 radical measurements in a polluted marine environment: links to ozone formation, *Atmos. Chem. Phys. Discuss.* 9 (**2009**), 24531–24585

10. Monks, P., et al.: Atmospheric composition change – global and regional air quality, *Atmos. Env. 43* (**2009**), 5268–5350

11. Muller, J. and Stavrakou, T.: Inversion of CO and NOx emissions using the adjoint of the IMAGES model, *Atmos. Chem. Phys.* 5 (**2005**), 1157–1186

12. Noxon, J., Norton, R. and Henderson, W.: Observation of atmospheric NO_3, *Geophys. Res. Lett.* 5 (**1978**), 675-679

13. Noxon, J., Norton, R. and Marovich, E.: Observation of atmospheric NO_3, *Geophys. Res. Lett.* 7 (**1980**), 125-128

14. Otten, C., Ferlemann, F., Platt, U., Wagner, T. and Pfeilsticker, K., Ground based DOAS UV/visible measurements at Kiruna (Sweden) during the SESAME winters 1993/94 and1994/95, *J. Atmos. Chem.* 30 (**1998**), 141-162

15. Platt, U., Perner, D. and Patz, H.: Simultaneous measurements of atmospheric CH2, O3 and NO2 by differential optical absorption, *J. Geophys. Res. 84* (**1979**), 6329–6335

16. Platt, U. and Perner, D.: Measurements of atmospheric trace gases by long path differential UV/visible absorption spectroscopy in Optical and Laser Remote Sensing, pp. 95-105, Springer Verlag, New York, (**1983**).

17. Platt, U.: Differential optical absorption spectroscopy (DOAS), *Chem. Anal. Series*, 127 (**1994**), 27 - 83

18. Platt, U. and Stutz, J.: Differential optical absorption spectroscopy – principles and applications, pp. 175-178, Springer Verlag, New York, (**2008**).

19. Rozenberg, G.: Twilight: A Study in Atmospheric Optics, p.160, New York: Plenum Press (**1966**)

20. Smith, J and Solomon, S.: Atmospheric NO_3. Sunrise disappearance and the stratospheric profile, *Geophys. Res.* 95 (**1990**), 13819-13827

21. Smith, J., Solomon, S., Sanders, R., Miller, H. and Perliski, L.: Atmospheric NO_3. Vertical profiles at middle and polar latitudes at sunrise, *Geophys. Res.* 98 (**1993**), 8983-8989

22. Stutz, et. al.: Nocturnal NO_3 Radical Chemistry in Houstan, TX, *doi: 10.1016/ J. Atmos. Env.* **2009**.03.004, 1-8

23. Solomon, S., Mount, G., Sanders, R. and Schmeltekopf, A.: Visible spectroscopy at McMurdo station, Antarctica: 2. Observation of OClO, J. Geophys. Res. 92 (**1987**), 8329-8338

24. Solomon, S., Sanders, R., Mount, G., Carrol, M. and Jakoubeka, R., Atmospheric NO_3 observations in polar regions: 2., *J . Geophys. Res.* 94 (**1989**), 16423-16427

25. Sommariva, R. et al.: Night-time radical chemistry during the NAMBLEX campaign, *Atmos. Chem. Phys. 7* (**2007**) 587–598

26. Wagner, T., Erle, F., Marquard, L., Otten, C., Pfeilsticker, K., Senne, T., Stutz, J. and Platt, U.: Cloudy sky optical paths as derived from differential optical absorption spectroscopy observations, *J. Geophys. Res.* 103 (**1998**), 25307-25321

27. Wagner, T., Otten, C., Pfeilsticker, K., Pundt, I. and Platt, U.: DOAS moonlight observations of NO_3 during the Arctic winter, *Geophys. Res. Lett.* 27 (**2000**), 3441-3444

28. Wang, S., Ackermann, R. and Stutz, J.: Vertical profiles of O3 and NOx chemistry in the polluted nocturnal boundary layer in Phoenix, AZ: I. Field observations by long-path DOAS, *Atmos. Chem. Phys.* 6 (**2006**), 2671–2693

29. Weaver, A., Solomon, S., Sanders, R. and Arpag, K.: Atmospheric NO_3. Off-axis measurements at sunrise: estimates of troposheric NO_3 at 40^oN, *Geophys. Res.* 101 (**1996**), 18605-18612

30. Yokelson, R., Burkholder, J., Fox, R., Talukdar, R. and Ravishankara, A.: Temperature dependence of NO_3 absorption spectrum, *J. Phys. Chem.* 98 (**1994**), 13144-13150

31. Young, A.: Air mass and refraction, *Applied Optics*. 33 (**1994**), 1108–1110

32. Yu, Y., Geyer, A., Xie, P., Galle, B., Limin, C. and Platt, U.: Observations of carbon disulfide by differential optical absorption spectroscopy in Shanghai, *Geophys. Res. Lett.* 31 (**2004**) l11107, doi: 10.1029/2004GL019543

33. Zingler, J. and Platt, U.: Iodine oxide in the dead sea valley: evidence for inorganic sources of boundary layer IO, *J. Geophys. Res* 110 (**2005**), doi: 10.1029/2004JD004993

Online Sources:

34. Yokelson (1994): NO_3 absorption cross section, *MPI-Maintz-UV-VIS Spectral Atlas of Gaseous Molecules*; http://www.atmosphere.mpg.de

35. Voight (2002): NO_2 absorption cross section, *MPI-Maintz-UV-VIS Spectral Atlas of Gaseous Molecules*; http://www.atmosphere.mpg.de

36. Moon data for Toronto, ON, Canada: http://www.timeanddate.com

37. Air Quality Ontario - Ministry of the Environment: http://www.airqualityontario.com/history/

38. York University ESSE Meteorological Observation Station: http://www.yorku.ca/pat/weatherStation/index.asp